Myeloperoxidase-dependent tyrosine halogenation potentiates α-defensins functions

Alessandro Foti[1], Robert Hurwitz[2], Kathrin Textoris-Taube[3], Michael Mülleder[4], Abin Biswas[5], Pauline Fahjen[1], Moritz Winkler[1], Ulrike Abu Abed[6], Daniel Humme[7], Stephanie Thee[8], Antje Prasse[9,10], Benjamin Seeliger [9,10], Markus Ralser[11] and Arturo Zychlinsky[1#]

[1] Department of Cellular Microbiology, Max Planck Institute for Infection Biology, Berlin 10117, Germany

[2] Protein Purification Core Facility, Max Planck Institute for Infection Biology, Berlin 10117, Germany

[3] Charité Universitätsmedizin Berlin, Department of Biochemistry, Core Facility - High-Throughput Mass Spectrometry 10117 Berlin, Germany

[4] Core Facility – High-Throughput Mass Spectrometry, Charité – Universitätsmedizin Berlin, Corporate Member of Freie Universität Berlin and Humboldt-Universität zu Berlin, Core Facility – High-Throughput Mass Spectrometry, Am Charitéplatz 1, Berlin, Germany

[5] Quantitative Biology, Max Planck Institute for Infection Biology, 10117, Berlin, Germany; Biological Optomechanics Division, Max Planck Institute for the Science of Light, Staudtstrasse 2, 91058 Erlangen, Germany

[6] Microscopy Core Facility, Max Planck Institute for Infection Biology, Chariteplatz 1, 10117 Berlin, Germany.

[7] Department of Dermatology, Venerology and Allergology, Charité Universitätsmedizin Berlin, corporate member of Freie Universität Berlin, Humboldt-Universität zu Berlin and Berlin Institute of Health, Berlin, Germany.

[8] Department of Pediatric Respiratory Medicine, Immunology and Critical Care Medicine, Charité-Universitätsmedizin Berlin, corporate member of Freie Universität Berlin, Humboldt-Universität zu Berlin, and Berlin Institute of Health, Berlin, Germany.

[9] Department of Respiratory Medicine, Hannover Medical School, Hannover, Germany.

[10] Biomedical Research in End-Stage and Obstructive Lung Disease (BREATH), Hannover Medical School (MHH), German Center for Lung Research (DZL), Hanover, Germany

[11] Charité Universitätsmedizin Berlin, Department of Biochemistry, 10117 Berlin, Germany; University of Oxford, The Wellcome Centre for Human Genetics, Nuffield Department of Medicine, Oxford OX3 7BN, United Kingdom;

[#] Corresponding author

Abstract

Neutrophils are immune cells specialized in detecting and eliminating microbes through potent cytotoxic mechanisms. Most of the neutrophil antimicrobial proteins are stored in intracellular organelles called granules, which are rapidly mobilized to direct the neutrophil cytotoxic machinery against the microbe. However, it remains unclear how the cytotoxic mechanisms cooperate with each other to minimize self-damage and allow an efficient immune response. Here we show that after neutrophil activation, highly oxidative myeloperoxidase-derived hypohalous acids target the antimicrobial peptides α-defensin 1-3, leading to chlorination of tyrosine 21 and iodination of tyrosine 16. We observe α-defensin 1-3 halogenation in rat neutrophils, and notably, in sputum samples from Cystic Fibrosis patients as well as in *Streptococcus pneumoniae* bronchoalveolar lavage (BAL) and *Staphylococcus aureus* skin abscesses infected patients. Importantly, halogenated α-defensins are more efficient immunomodulators and anti-toxin mediators than the non-modified peptides, indicating that this rare post-translational modification is important for inflammation.

Introduction

Neutrophils are the most abundant leukocytes in the bloodstream of humans and exert essential roles in microbes killing, immune regulation and surveillance. Neutrophils kill microbes trough two different strategies, traditionally known as oxidative and non-oxidative mechanisms [1]. Oxidative killing mechanisms include the formation of reactive oxygen species (ROS) generated by the NADPH oxidase (NOX2) and myeloperoxidase (MPO) [2]. Trough one-electron reduction of molecular oxygen, NOX2 generates large quantities of superoxide anion ($O2^{\bullet-}$), the precursor of most ROS. Superoxide anion dismutates to hydrogen peroxide (H_2O_2), which is converted by MPO together with halide ions (chloride, bromide, iodide or the pseudo-halogen thiocynite) to highly reactive hypohalous acids (HOX). Due to elevated bioavailability in tissues, the physiological halogen substrate of MPO is accepted to be chloride, which is enzymatically converted to hypochlorous acid (HOCl), a strong oxidant and chlorinating agent. In contrast, iodide is not considered a relevant *in vivo* substrate due to low concentration in biological tissues (<0.1 μM) compared to chloride (80-120 mM) [3]. ROS are essential in signaling and homeostasis, as well as during infectious and inflammatory diseases. Indeed, patients who are fully deficient in NOX2 or MPO activity are susceptible to recurrent infections and suffer from autoinflammation [2].

On the other hand, the non-oxidative neutrophil killing mechanisms instead include numerous proteases, antimicrobial peptides and enzymes. Particularly relevant are serine proteases as neutrophil elastase and cathepsin G, and the antimicrobial peptides like cathelicidins and α-defensins. Individuals deficient or hypomorphic of these proteins suffer from a range of different diseases [4].

A major question in neutrophil biology remains how different antimicrobial mechanisms are coordinated. Experimental and *in silico* evidence suggest that, during neutrophil activation, numerous antimicrobial proteins and ROS are released simultaneously at high concentrations (up to millimolar range) in narrow intracellular spaces, such as the phagolysosome or NETotic intracellular membrane-bound vacuoles [1,2]. Previous studies indicate that during early neutrophils activation, antimicrobial components act in close proximity and firstly interact with each other before targeting microbes [5]. Interestingly, during *Staphylococcus aureus* phagocytosis, MPO-derived hypohalous acids modify primarily neutrophil proteins, rather than bacterial proteins [6,7]. One possible explanation of these observations is that neutrophils could use protein halogenation

as a posttranslational modification to regulate immune responses. Here we show that in activated neutrophils, MPO chlorinates and iodinates the antimicrobial peptide α-defensin 1-3 (HNP1-3). HNP1-3 are three slightly cationic and hydrophobic peptides encoded from two genes DEFA1 and DEFA3, which code respectively for HNP1-2 and HNP3. HNP1-3 are 29-30 amino acids peptides distinguished only by the amino acid in position 1: HNP1 harbors an alanine residue, HNP2 none and HNP3 an aspartic acid [8]. We demonstrate that α-defensin1-3 are chlorinated on tyrosine 21 (ClY21-HNP1) and iodinated on tyrosine 16 (IY16-HNP1). Mice do not carry the genes encoding defensins [9], however, rats (*Rattus norvegicus*) express HNP1-3 homologs of the human HNP1-3 [10] and constitute a very promising animal model to study these peptides. We show that rat neutrophils, up on activation, also halogenated HNP1 on a conserved tyrosine residue. Notably, halogenated HNP1-3 are abundant in sputum from Cystic Fibrosis (CF) as well as in bronchoalveolar lavage (BAL) of patients infected with *S. pneumoniae* and in abscesses of patients infected with *S. aureus*. Halogenated HNP1s were more effective immunomodulators and displayed strong anti-toxin activity than unmodified HNP1. We propose that the novel HNP1-3 post-translational halogenation is the result of a cooperative event interconnecting the oxidative and non-oxidative antimicrobial mechanisms in neutrophils.

Results

Human neutrophils halogenate alpha-defensin 1-3

Upon activation, neutrophils generate high amount of reactive oxygen species (ROS) and hypohalous acids (HOX). We incubated freshly blood-isolated human neutrophils with 3′-(p-aminophenyl)-fluorescein (APF), a reporter sensing the MPO-derived HOX, and then stimulated them with *S. aureus* or phorbol myristate acetate (PMA). Optical diffraction tomography (ODT) in combination with confocal microscopy showed significant amount of HOX accumulated within intracellular phagolysosomes or membrane-bound vacuoles (Fig. 1a). As expected, the NOX2 inhibitor diphenyl-iodonium (DPI) or the MPO inhibitor 4-sminobenzoic hydrazide (4-ABAH) significantly reduced the APF fluorescence on stimulated neutrophils (Fig. S1).

To test our hypothesis, we stimulated human neutrophils using PMA, *S. aureus* or zymosan beads, then isolated the total proteins and measured the percentage of 3-chloro-tyrosines (ClY), a stable

HOCl-derived modification, by acid-hydrolysis and mass spectrometry (ESI-MS). PMA, *S. aureus* and zymosan beads induced an increase to 3.3, 1.7 and 1.9 % of chloro-tyrosine/total tyrosine ratio, respectively (Fig. 1b). To confirm that the chloro-tyrosines were protein-bound and not the result of protein fragmentation after cell stimulation, we measured the level of free chloro-tyrosines from neutrophils by ESI-MS without performing the hydrolysis step. Our data show that the vast majority of the chloro-tyrosines observed were protein bound (Fig. S2). To identify the proteins harboring chloro-tyrosines, we stimulated freshly isolated neutrophils with PMA or *S. aureus* and fractionated the total neutrophil proteome by ammonium sulphate (AS) precipitation (Fig. 1c). The AS fractions were analyzed by SDS-PAGE and LC-MS proteomics. Intriguingly, the fraction 1, of either PMA or *S. aureus* stimulated cells, contained >90% of the chloro-tyrosines (Fig. 1d-e). Mass spectrometry analysis showed that the most abundant protein in fraction 1 was the antimicrobial peptide α-defensin1-3 (HNP1-3) (Fig. 1f).

To identity the major chlorinated proteins, we labeled neutrophils in custom cell culture medium enriched with NaCl containing the radioactive isotope ^{36}Cl for 1 h before activation with PMA or *S. aureus*. After 1 h stimulation, cell lysates were separated by SDS-PAGE and subjected to autoradiography. Interestingly, we detected only one major band at around 10 KDa (Fig. 1g). We confirmed by mass spectrometry that the most abundant protein in the gel band was HNP1-3 (Fig. 1h). We further analyzed the total proteome of activated neutrophils by LC-MS/MS label free quantification (LFQ) and intensity Based Absolute Quantification (iBAQ), using the MaxQuant analysis software and searched for halogenated tyrosine containing peptides [11]. We performed a Tricine 16% SDS-PAGE to resolve the low molecular weight proteins and examined the levels of halogenate peptides in the gel bands by mass spectrometry (Fig. 1i). The results confirmed that the most abundant chlorinated peptide was present in band 2 and contained a HNP1-3-derived peptide (Y-G-T-C-I-Y-Q-G-R), harboring chlorination on tyrosine in position 21 (Fig. 1j). Twenty percent of chlorinated HNP1-3-derived peptide contained the chloro-tyrosine in position 16 (Fig. 1j). Notably, we also found that α-defensin1-3 was tyrosine iodinated in position 16 (80%) and position 21 (20%) (Fig. 1k). Moreover, neutrophils preincubated with sodium iodide (100 μM) displayed a 5-fold decrease in HNP1-3 chlorination and 10-fold increase in HNP1-3 iodination (Fig. S3). Either chlorination or iodination of HNP1-3 was greatly reduced by the MPO inhibitor 4-aminobenzoic acid hydrazide (4-ABAH) (Fig. S4). Notably, no tyrosine bromination was detected

on HNP1-3 based on our analysis, even after preincubation of neutrophils with extra sodium bromide (100 μM) (Fig. S3).

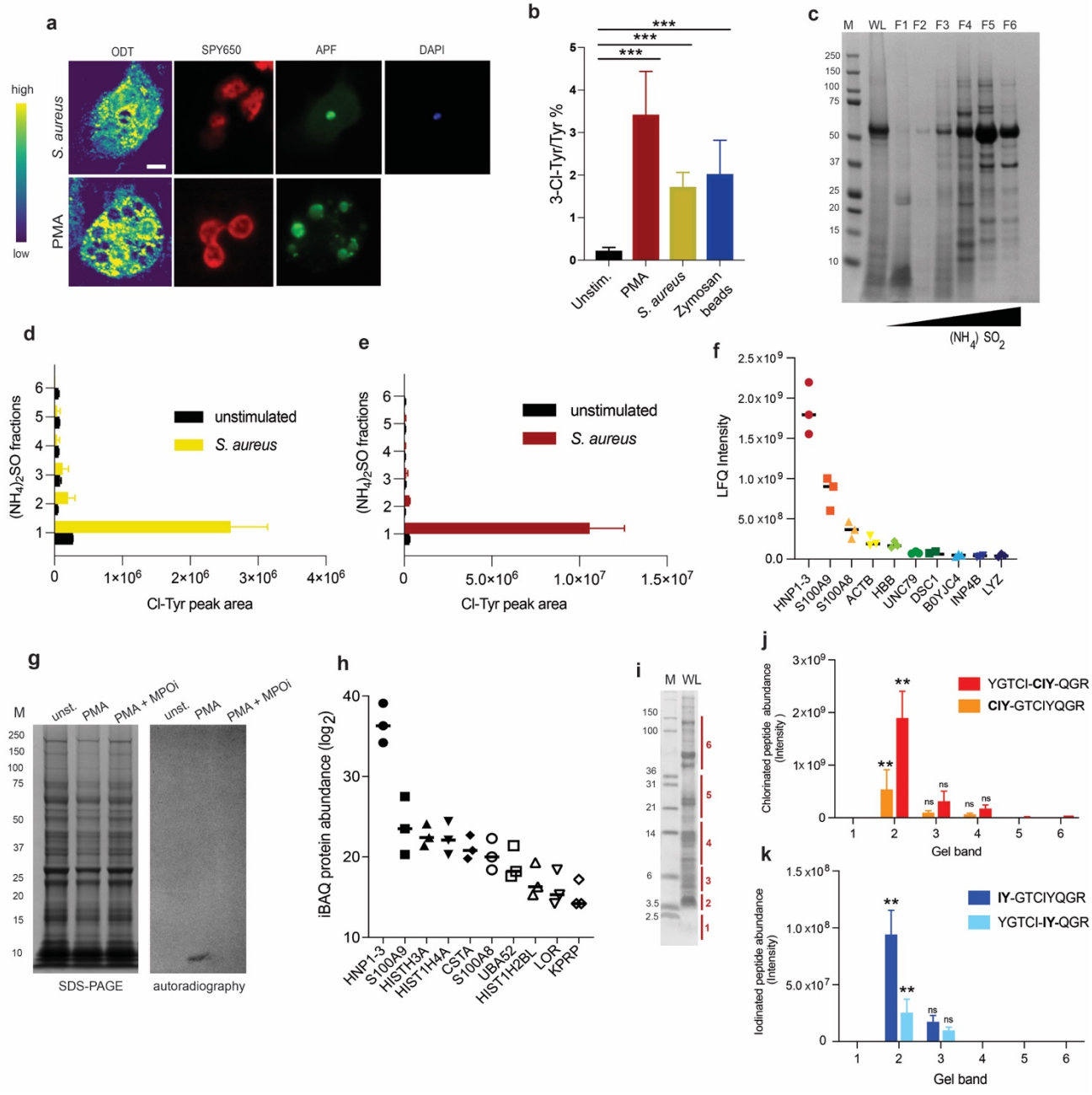

Figure 1. Human neutrophils halogenate HNP1-3. Representative optical diffraction tomography (ODT) and confocal microscopy images of phagocytic and pharmacologically activated human neutrophils generating hypohalous acids. SPY650-DNA, neutrophils chromatin; APF, hypohalous acids; DAPI, bacterial cells. Scale bar, 2 µm. Color bar on left shows the density distribution (a). Ratio of total 3-Cl-Tyr/Tyr analyzed by acid hydrolysis and ESI-MS. Bars show means ± SEM, n = 5. ***p < 0.001, unpaired Student's t test (b). SDS-PAGE of ammonium sulphate precipitation fractions of activated human neutrophils, n = 3 (c). Cl-Tyr quantification of the ammonium sulphate fractions of neutrophils activated with *S. aureus* (d) or PMA (e). Bars show means ± SEM, n = 4. Label-free proteomic quantification of the proteins in fraction 1, n = 3 (f). ^{36}Cl radio-labelling of human neutrophils unstimulated, activated and in presence of MPO inhibitor (4-ABAH), SDS-PAGE (left) and autoradiography (right), n = 6 (g). Proteomic analysis of the radio-labelled band from Fig. A g, n=3 (h). Tricine 16% denaturating acrylammide gel of human neutrophils cell lysate, n=3 (i). Proteomic analysis of gel bands and quantification of chlorinated (j) and iodinated (k) HNP1-3 derived peptides from tricine gel 16%. Bars show means ± SEM, n = 3. **p < 0.01, ns, non-significant unpaired student's t test.

Rat neutrophils halogenate α-defensins homologs

To test whether MPO-dependent HNP1-3 halogenation is conserved, we measured it in three additional cell types: (1) human monocytes, which express MPO, but not significant levels of HNP1-3, (2) mouse neutrophils, which express MPO but lack the genes encoding HNP1-3 and (3) rat neutrophils, which express MPO and HNP1-3 homologs, thus resembling human neutrophils. Firstly, we measured hypohalous acids formation using the APF reporter after stimulation with *S. aureus* or by adding exogenous hydrogen peroxide to directly activate MPO. All four MPO-expressing cell types produced significant levels of HOX (Fig. 2a).

We isolated the total proteome from the four cell types and analyzed the halo-tyrosine levels by acid hydrolysis and ESI-MS. Interestingly, we detected significant levels of chloro-tyrosine only in human and rat neutrophils, cells that express both MPO and HNP1-3 (Fig. 2b). Rat neutrophils express the HNP1-3 homologs, neutrophil peptide 1-3 (rNP1-3). Human and rat NP1 share 44% amino acid sequence identity and 53% similarity and display a high degree of structural organization based on *in silico* analysis (Fig. 2c). To confirm our results, we purified rat neutrophils from peripheral blood by an antibody-based negative selection method, infected them with *S. aureus* and showed, by immunofluorescence that the engulfed bacteria are surrounded by RNP1-3 and MPO (Fig. 2d). Subsequently, we measured the overall proteome in rat neutrophils infected with *S. aureus* or stimulated with hydrogen peroxide by LC-MS/MS proteomics and found chlorination of the LSGACG-ClY-RG peptide. Interestingly, this peptide corresponds to the rat HNP1-3 homolog NP1 (Fig. 2e). Importantly, chlorination of rat NP1 (Fig. 2f), like in HNP1-3 (Fig. 1j), occurred on the tyrosine residue 21, which is a structurally conserved target between rats and humans.

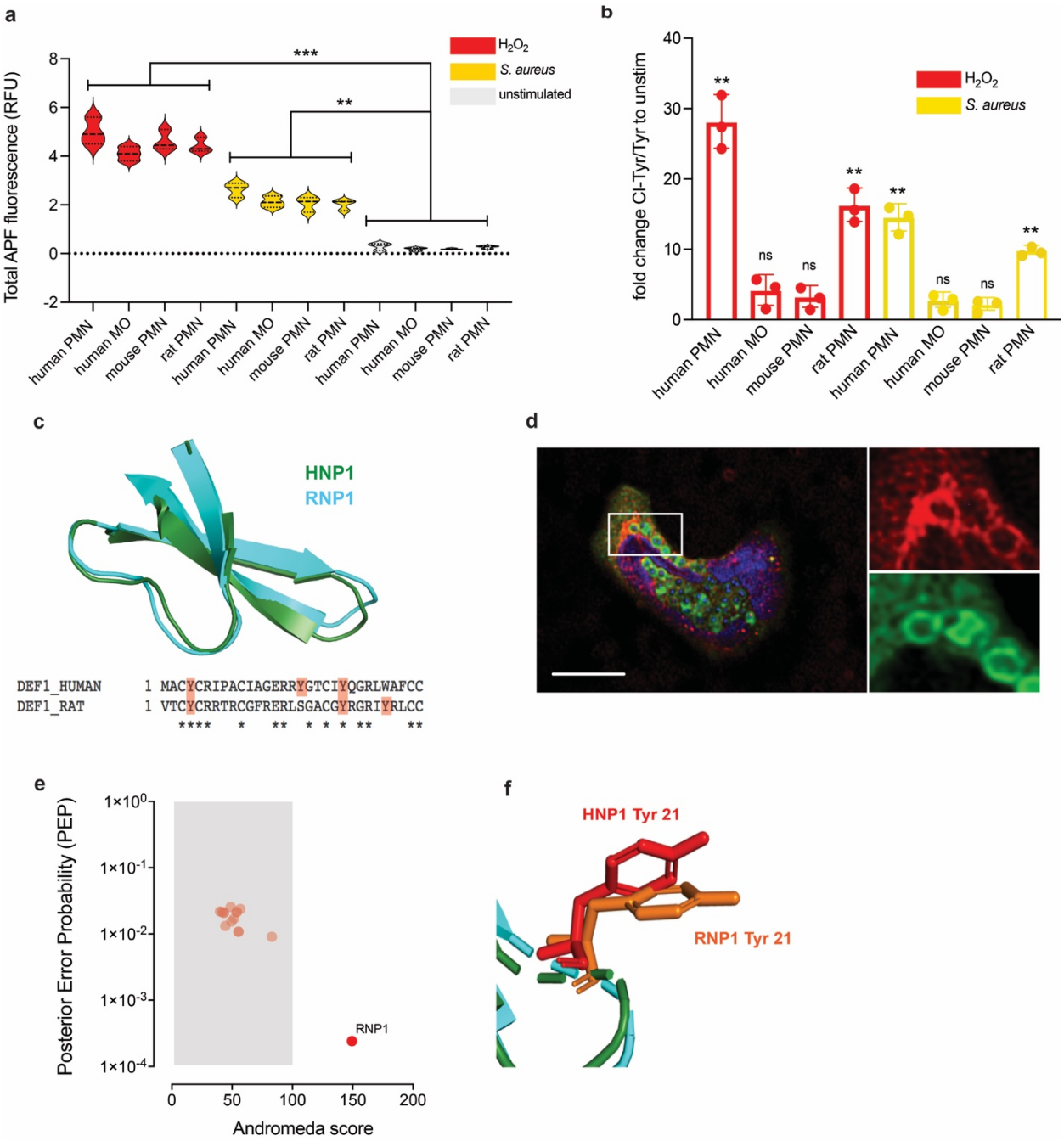

Figure 2. Rat neutrophils halogenate HNP1 homolog. Human neutrophils, human monocytes, mouse neutrophils and rat neutrophils were stimulated with H_2O_2 and *S. aureus* to produce hypohalous acids and measured by APF fluorescence. Bars show means ± SEM, n = 3. ***p < 0.001, **p < 0.01, ns, non-significant unpaired student's t test (a). Chlorotyrosine levels of human neutrophils, human monocytes, mouse neutrophils and rat neutrophils were stimulated with H_2O_2 and *S. aureus*. Bars show means ± SEM, n = 3. ***p < 0.001, **p < 0.01 ns, non-significant unpaired student's t test (b). Superimposed 3D-structure of HNP1 (PDB:1gny) and RNP1 (AF-Q62716-F1-model_v2) and amino acid alignment generated with PyMOL Molecular Graphics System (c). Representative confocal microscopy image of isolated rat neutrophil stimulated with *S. aureus* and stained for MPO (green) and RNP1-3 (red). Cells were stained with DAPI to visualize DNA (blue). Scale bar, 2 µm. n=3 (d). Mass spectrometry analysis of halogenated rat peptides, n = 3 (e). Superimposition of the 3D-structure of HNP1 Tyr21 (PDB:1gny) and RNP1 Tyr 21 (AF-Q62716-F1-model_v2) and amino acid alignment generated with PyMOL Molecular Graphics System (f).

Cystic fibrosis, *S. pneumoniae* and *S. aureus* infected patients generate halogenated HNP1-3

We confirmed tyrosine halogenation of HNP1-3 in pathological samples from three different sources: sputum of CF patients as well as BAL from patients infected with *S. pneumoniae* and patient with a *S. aureus* skin infection. We analyzed sputum from CF patients which are characterized by a high neutrophil infiltration into the lungs [12] by LC-MS/MS. We observed the highest level of chlorination on Tyr 21 and iodination on Tyr16 of HNP1-3 (Fig. 3a). Of note, we observed tyrosine chlorination on other proteins, like transmembrane channel 4, SLC25 and BAZ2A albeit in minor amounts. Beside HNP1-3, other proteins were significantly iodinated, such as Calprotectin (S100A8/A9), lysozyme (Lyz) and histone 4 (H4). We investigated skin abscesses from patients infected with *S. aureus* which also attract neutrophils. As observed with CF samples, *S. aureus* infected patients generated significant amounts of halogenated HNP1-3 (Fig. 3b). Like in CF patients, Tyr 21 and Tyr 16 where the most abundant chlorinated and iodinated residues respectively, in HNP1-3. The other halogenated proteins were also similar to those observed in samples from CF patients. Interestingly, we also found chlorination on Tyr 3 of a HNP1-3-derived peptide (NMAC-ClY-CRIPACIAGERR). As control, we analyzed the tissue neighboring the abscess, where we did not detect halogenated proteins. Lastly, we analyzed BAL samples from *S. pneumoniae* infected patients hospitalized in the intensive care units (ICU), which confirmed the presence of chlorinated Tyr 21 and iodinated Tyr 16 on HNP1-3 (Fig. 3c). Altogether these data demonstrate the HNP1-3 halogenation occurs *in vivo* in humans.

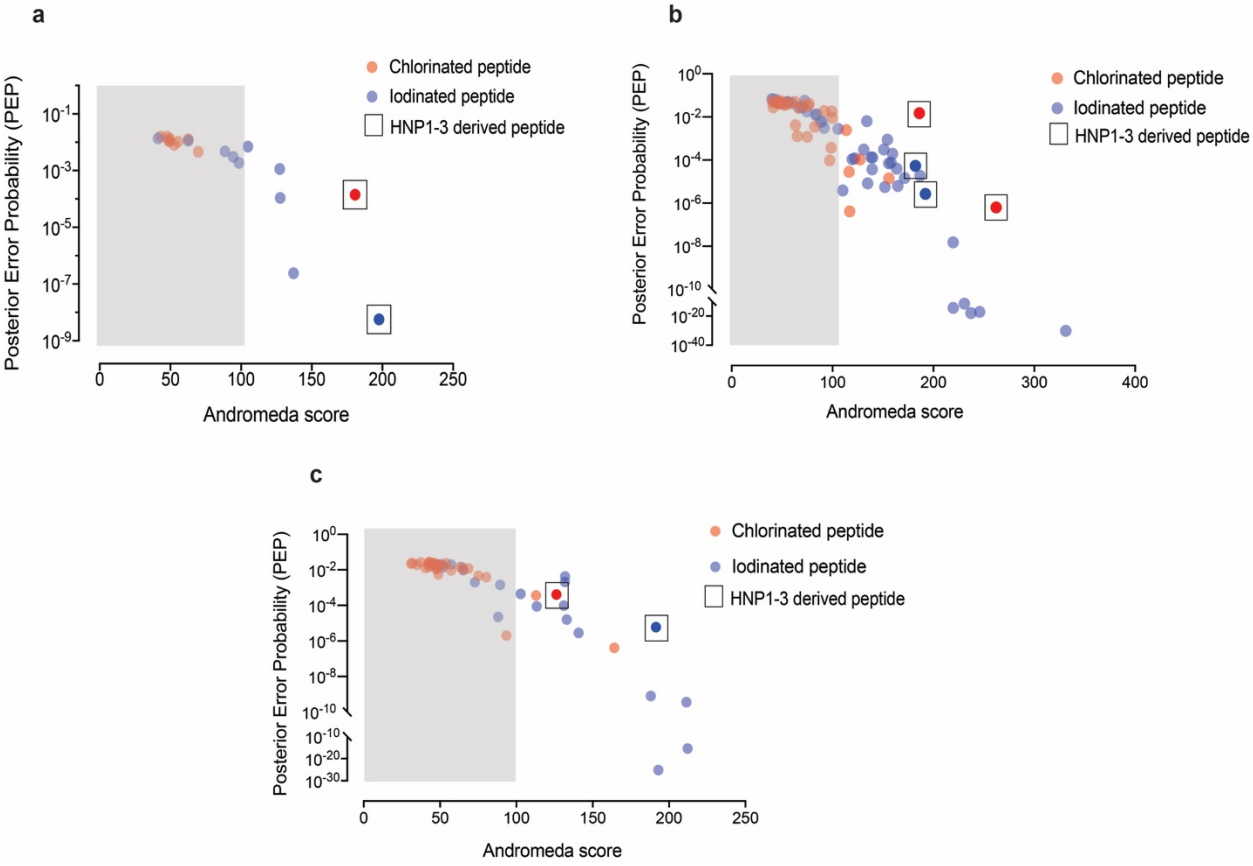

Figure 3. CF, *S. pneumoniae* and *S. aureus* infected patients generate halogenated HNP1-3. Liquid-Chromatography Mass spectrometry (LC-MS/MS) analysis of CF patients (n=3) sputum samples analyzed for chlorinated and iodinated proteins (a); *S. aureus* skin infected patients (n=2) samples were analyzed for chlorinated and iodinated proteins (b); *S. pneumoniae* infected patients (n=4) BAL samples were analyzed for chlorinated and iodinated proteins (c). Each red and blue point indicates respectively a chlorinated and iodinated HNP1-3 derived peptide. Squares indicate HNP1-3 derived peptides.

Halogenation modifies the physicochemical properties of HNP1-3

Tyrosine halogenation is a stable modification that affects the physicochemical properties of proteins and large-scale protein self-organization [13]. Covalently bound chlorine and iodine may alter the tyrosine hindrance sphere surrounding the tyrosyl group and therefore modulate its electrochemical properties. Interestingly, the tyrosine residues 16 and 21 coordinate two hydrophobic regions of HNP1-3, called hydrophobic pockets 1 and 2, through interaction with the residues phenylalanine 28 and tryptophan 26 (Fig. 4a). HNP1-3 are short peptides containing only 29-30 amino acids [7] and the short size of these peptides makes them suitable for chemical synthesis [14]. To test the significance of tyrosine halogenation of HNP1-3, we synthetized halogenated HNP1 variants and compared their physicochemical properties to the unmodified peptide. Ultra-pressure

liquid chromatography (UPLC) using a C18-reverse phase column showed that halogenated HNP1 elute after the unmodified HNP1, indicating an increase in hydrophobicity (Fig. 4b). Halogenated HNP1 also showed higher Nile Red binding than unmodified HNP1 in spectrofluorometric measurements, indicating, again an increase in hydrophobicity (Fig 4c).

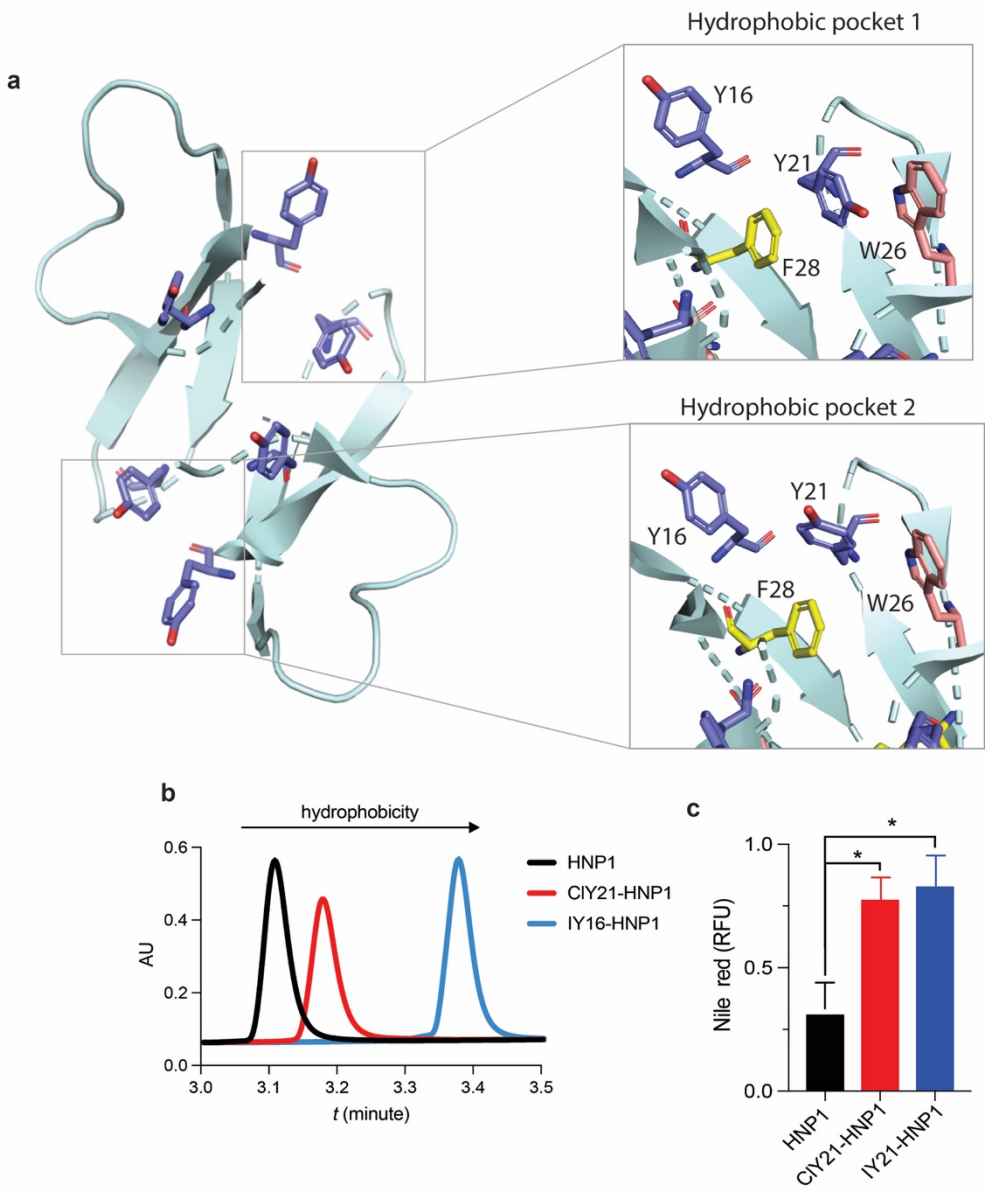

Figure 4. Halogenation modifies the physicochemical properties of HNP1-3. 3D-structure of HNP1 and spatial organization of the hydrophobic pocket 1 and 2 with the corresponding amino acids (PDB:1gny) generated with PyMOL Molecular Graphics System (a); Ultra pressure liquid chromatography (UPLC) using C18-reverse phase column analysis of HNP1, ClY-21-HNP1 and IY16-HNP1 n=3 (b). Nile red fluorescence measure from HNP1, ClY-21-HNP1 and IY16-HNP1. Bars show means ± SEM, n = *3*. *p < 0.01, unpaired Student's t test (c).

Halogenation increases the chemokine activity of HNP1

Subsequently, we tested whether chlorination and iodination influence HNP1 functions. Halogenation did not affect killing of *S. aureus* (Fig. 5 a), *Escherichia coli* or *Candida albicans* (Fig. S5) in hypotonic medium, the condition known to allow cytotoxic properties of HNP1-3 [15]. Notably, HNP1-3 are chemotactic to immune cells in isotonic medium, a more physiological condition [16,17]. Using a transwell migration assay (Boyden chamber) with a pore size of 3 µm for neutrophils (Fig. 5 b) or 5 µm for monocytes (Fig. 5 c) we found that halo-HNP1s are a more potent chemoattractant than unmodified HNP1. Indeed, halo-HNP1 was as effective as the control chemoatractants, fMLP for neutrophils and chemotactic protein 1 (CCL2) for monocytes (Fig. 5b). Interestingly, IY16-HNP1was 6-fold and 2-fold more effective in neutrophils and monocytes respectively, compared to unmodified HNP. In contrast, DTT-unfolded halo-HNP1 did not induce chemotaxis of either cell.

Subsequently, we pretreated human monocytes derived macrophages (HMDM) with HNP1s or vehicle for 1 h and then stimulated them with *S. aureus* (MOI 1:10) for 3 h. We used the supernatant to measure cytokine production with a membrane-based antibody array. Halo-HNP1 induced a stronger production of MCP-1 (CCL2), MCP-1α (CCL3) and MCP-1β (CCL4) than HNP1 (Fig. S5). These proteins are chemotactic to immune cells, in particular monocytes. Interestingly, halo-HNP1s induced a slight production of CCL2, CCL3 and CCL4 even in the absence of *S. aureus* infection. Additionally, halo-HNP1 upregulated production of IL-18 binding protein (IL-8bp), an anti-inflammatory cytokine inhibiting IL-8 downstream effects. We quantified cytokines and chemokines by ELISA and found that halo-HNP1 induce higher release of CCL2 and CCL3 and CCL4 than unmodified peptide, respectively (Fig. 5 d-e). A slight increase of these chemokines was observed also in non-infected HMDM in presence of halo-HNP1s, and in case of CCL4 we observed an increase with unmodified HNP1 (Fig. S5).

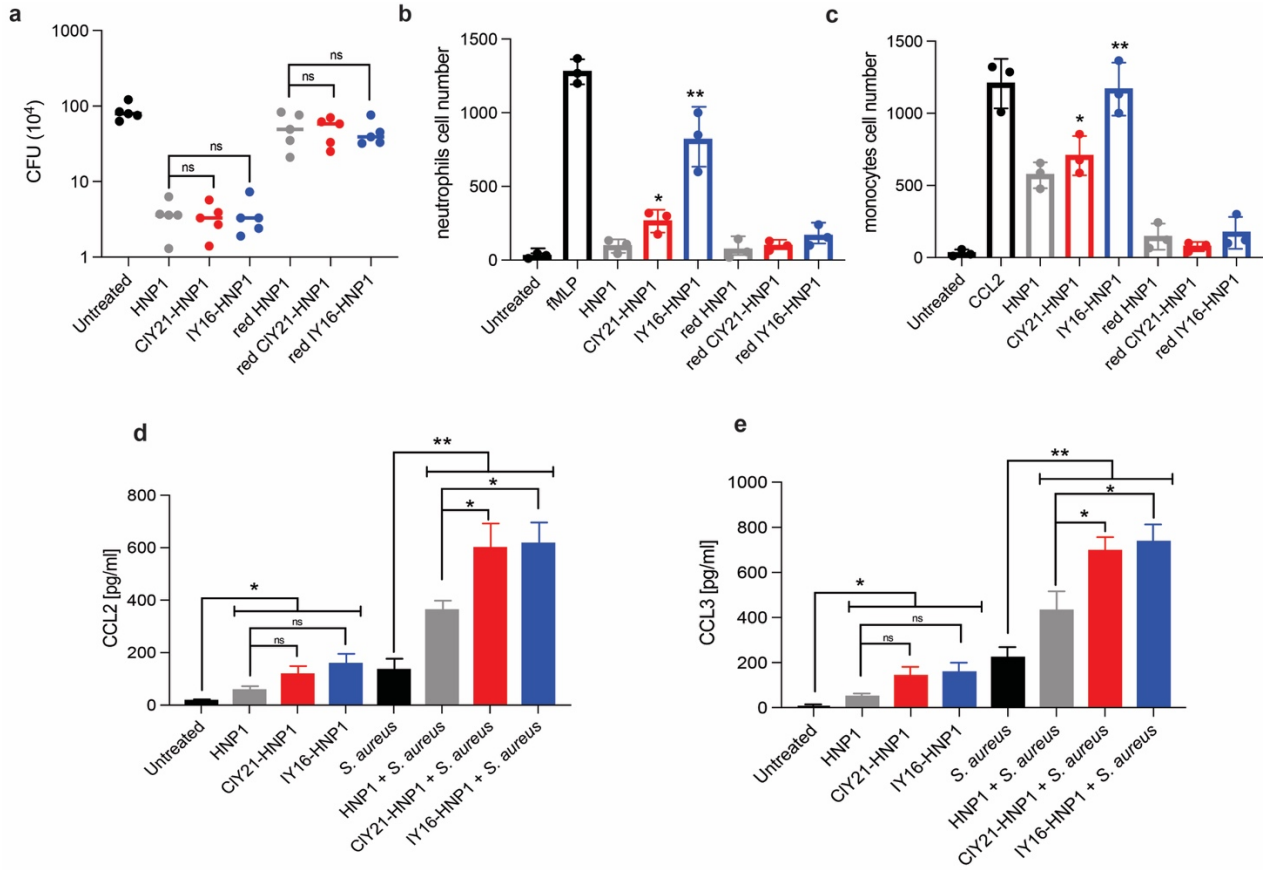

Figure 5. Halogenation increases the chemokine activity of HNP1. *S. aureus* killing assay using HNP1, ClY-21-HNP1 and IY16-HNP1(50 µg/ml), and denaturated (reduced) peptides as control. Bars show means ± SEM, n = 3., ns, non-significant unpaired Student's t test (a). Chemotaxis assay of human neutrophils (b) and monocytes (c). Bars show means ± SEM, n = 3. **p < 0.001, *p < 0.01, ns, non-significant unpaired Student's t test. ELISA of HMDM infected with *S. aureus* and treated with HNP1, ClY-21-HNP1 and IY16-HNP1 (10 µg/ml) to detect levels of CCL2 (d) and CCL3 (e). Bars show means ± SEM, n = 3. **p < 0.001, *p < 0.01, ns, non-significant unpaired Student's t test.

Anti-toxin activity of HNP1 is potentiated by halogenation

HNP1-3 can act as anti-chaperone to bacterial toxins, by binding hydrophobic regions of the target and unfolding it [18]. Molecular dynamics studies showed that the anti-chaperone activity of HNP1-3 is driven by their hydrophobic regions, in particular the hydrophobic pockets 1 and 2, coordinated by the residues Tyr 16, Tyr 21, Trp 26 and Phe 28 (Fig. 4 a). The proposed mechanism poses that defensin dimers loosely bind to the surface of toxins and increase the local instability by rearranging hydrophobic interactions from homo-molecular (monomer-monomer) to plausibly more potent heteromolecular (monomer-toxin), between dissociated defensin monomers and exposed hydrophobic regions of the toxin [19].

Based on these observations, we tested the toxin inhibition activity of halo-HNP1s and unmodified peptide against several bacterial toxins. In thermostability studies we showed that halo-HNP1 unfolds the *Bacillus anthracis* toxin Lethal Factor (LF) more effectively than unmodified HNP1 (Fig. 6a). LF is a zinc-binding metalloprotease that cleaves MAP kinases after entering immune cells. Furthermore, we used N-acetylated, C-7-amido-4-methylcoumarin (AMC) derivative of a 14-mer peptide substrate designed from the MEK-2 template to measure LF proteolysis. This assay showed that halo-HNP1, in particular the chlorinated Tyr 16 variant, inhibited the LF proteolityc activity more effectively than the unmodified HNP1 (Fig. 6b).

To confirm the anti-toxin activity, we measured cell death in RAW 264.7 macrophages intoxicated with holo-Anthrax toxin in the presence of HNP1s. Microscopic analysis showed that halo-HNP1 protected cells better than the unmodified peptide (Fig. 6c). Quantification with lactate dehydrogenase (LDH) release showed that HNP1 chlorination potentiated the antitoxin activity 10 folds and the iodination by 8 folds compared to the unmodified HNP1 (Fig. 6d). Interestingly, unmodified as well as halo-HNP1s do not inhibit human proteases like neutrophil elastase, cathepsin G or metalloproteinase 8 (data not shown), suggesting a degree of specificity toward bacterial toxins. We also incubate the toxin with LL37, a neutrophil cationic peptide, that does not have a known anti-toxin activity as a control (Fig. 6d). Lastly, to extend these findings, we demonstrated the anti-chaperone activity of halo-HNP1 on Lysteriolisin O (LLO) from *Listeria monocytogenes*, Pneumolysin (PLY) from *S. pneumoniae* and Panton-Valentine leukocidin (PVL) from *S. aureus*. LLO (Fig. 6e) and PLY (Fig. 6f) activity was measured by erythrocytes lysis, followed by change in optical density at 700 nm. Both LLO and PLY activity was more susceptible to halo-HNP1s than to the unmodified defensin. Furthermore, halo-HNP1s were highly effective than the unmodified peptide in reducing the toxicity of PVL on human neutrophils (Fig. 6g).

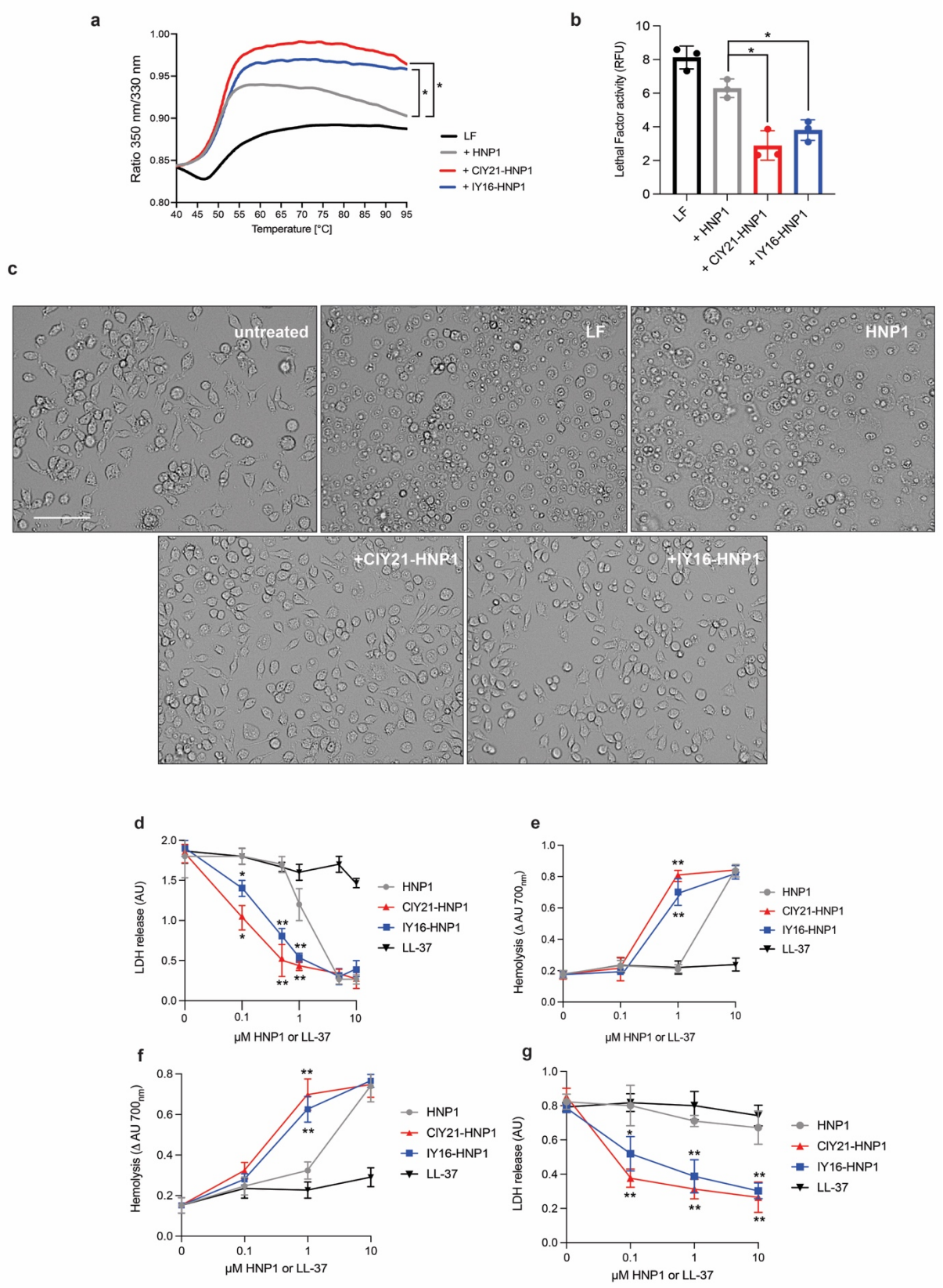

Figure 6. Anti-toxin activity of HNP1 is potentiated by halogenation. Thermostability assay of Lethal Factor (LF) binding to HNP1, ClY-21-HNP1 and IY16-HNP1. n=3. *p < 0.01, unpaired Student's t test (a); Proteolytic measurement by fluorogenic substrate of LF (20 nM) in presence of HNP1, ClY-21-HNP1 and IY16-HNP1 (1µM). Bars show means ± SEM, n = 3. *p < 0. 01, unpaired Student's t test. (b); Representative images of RAW 264.7 macrophages intoxicated with LF (20 nM) and/or treated with HNP1, ClY-21-HNP1 and IY16-HNP1 (1µM). Scale bar, 50 µm, n=5 (c). Cytotoxicity measurement of RAW 264.7 macrophages infected with LF. Data points show means ± SEM, n = 3. *p < 0.01, **p < 0.001 unpaired Student's t test (d); Hemolysis assay measurement of LLO activity and anti-toxin activity of HNP1, ClY-21-HNP1 and IY16-HNP1. Data points show means ± SEM, n = 3. *p < 0.01, **p < 0.001 unpaired Student's t test (e). Hemolysis assay measurement of PLY activity and anti-toxin activity of HNP1, ClY-21-HNP1 and IY16-HNP1. Data points show means ± SEM, n = 3. *p < 0.01, **p < 0.001, unpaired Student's t test (f); Cytotoxicity measurement of human neutrophils infected with PVL toxin and anti-toxin activity of HNP1, ClY-21-HNP1 and IY16-HNP1. Data points show means ± SEM, n = 3. *p < 0.01, **p < 0.001 unpaired Student's t test. Bars show means ± SEM, n = 3. *p < 0.01; **p < 0.001 ns, non-significant unpaired Student's t test.

Discussion

Neutrophils are immune cells specialized in rapidly recognizing, killing and degrading invading microbes. The neutrophil antimicrobial machinery is extremely cytotoxic and need to be tightly regulated to avoid tissue damage. When neutrophils are not effective, the host suffers from recurrent infections and where they are overactive induce inflammatory diseases [20]. These cells possess multiple antimicrobial mechanisms, often redundant or overlapping, which are conventionally categorized in two major groups: oxidative and non-oxidative mechanisms.

The oxidative mechanisms consist of ROS and hypohalous acids (HOX) generated respectively from the NADPH oxidase (NOX2) and the heme-dependent enzyme myeloperoxidase (MPO) [2]. H_2O_2 is the substrate of MPO, which sequentially generates HOX. The non-oxidative branch includes proteases, antimicrobial peptides and other antimicrobial proteins stored in intracellular organelles called granules. Even though neutrophil antimicrobial proteins are stored and activated within the same intracellular organelles, and therefore act in close proximity to each other, it remains unclear whether these mechanisms interact during neutrophil activation.

Here we report a new synergistic mechanism between the oxidative and non-oxidative neutrophil antimicrobial systems. We show that, during neutrophil activation, the MPO-derived hypohalous acids (hypochlorous and hypoiodous acid), post-translationally modify the antimicrobial peptides HNP1-3, chlorinating and iodinating mainly Tyr 21 and Tyr 16. These data suggest that neutrophils generate significant amount of hypoiodous acid (HOI), which was previously excluded as physiologically relevant MPO product due low concentration of iodide in biological tissues [3]. This information is relevant because HOI is demonstrated to be around 100 fold more potent than HOCl

in killing bacterial pathogens [21], indicating a direct role for iodide in containing infections. The role of iodide in extra-thyroid functions was previously investigated [22] and a partial iodine deficiency (urinary excretion of 4 mg/day) was enough to ensure normal thyroid functionality, but it coincides with severe alterations in the immune response of children [23]. Interestingly, iodide supplementation (2 mg/week) for 8 months restored the immune response [23]. Our data suggest that neutrophils can import significant amount of iodide into their compartments, despite the low abundance of this halogen in tissues, and confirm their iodide ion influx capacity demonstrated *in vitro* [24].

Halogens are highly reactive elements that are essential for life. Chloride, bromide, iodide and the pseudo-halogen thiocyanate are particularly important in immunity [25]. Biological halogenation was first described on the thyroid gland in the early 1900´s, and later thyroglobulin was shown to be heavily iodinated in order to generate the thyroid hormones triiodothyronine (T3) and thyroxine (T4) [26]. Subsequently, other cases of biological halogenation in humans were discovered, as chlorination of Apolipoprotein 1 in atherosclerotic plaques [27] and bromination of Collagen IV, which regulates the extracellular matrix organization [28]. Additionally, cell-free tyrosine chlorination was shown to modify protein functions *in vitro* [29,30]. In microbiology, protein halogenation occurs in fungi and bacteria, mainly catalyzed by chloroperoxidases and vanadium peroxidases [31]. Interestingly, N-chlorination, a reversible form of halogenation, was shown to occur on a bacterial chaperone involved in oxidative stress response [32]. Chemical halogenation of the antimicrobial peptide Jelleine-I, a peptide originally isolated from the royal jelly of honeybees (*Apis mellifera*), was shown to increase antimicrobial activity and higher resistance to proteolytic cleavage of the peptide [33]. As far as we know, iodinated HNP1-3 is the first characterization of a biologically iodinated protein in humans under pathophysiological conditions. Notably, in humans, iodothyronine deiodinases (DIO1, DIO2 and DIO3) and iodotyrosine deiodinase (IYD) are selenium-containing enzymes that catalyze the release of iodide from thyroid hormones (DIOs) and directly from iodo-tyrosines (IYD), modulating iodide metabolism and thyroid hormonal regulation [34]. Further studies will be needed to test whether deiodinase enzymes are able to deiodinate HNP1-3 peptides. Up to now, there are no tyrosine de-chlorinating enzymes reported in humans.

Our data show that significant levels of tyrosine halogenation occurs in cells that express MPO and α-defensins. Interestingly, human monocytes and mouse neutrophils, both expressing active

MPO but not α-defensins, and generating high amounts of HOX, did not produce comparable levels of ClY to human and rat neutrophils. These data indicate an unexpected specificity of the MPO-dependent halogenation mechanism, which preferentially targets and post-translationally modifies α-defensins during neutrophil activation. Rat defensins are valuable models to study HNP1-3 because of their high similarity to the human peptides. Notably, α-defensins halogenation was observed in human and rat neutrophils on the conserved tyrosine residue in position 21.

Importantly, we observed significant levels of halo-HNP1-3 in samples from CF patients, a disease characterized from persistent inflammation in the lung, where massive number of neutrophils generate ROS. Interestingly, CF neutrophils were shown to generate less HOCl compared to healthy donors due to impaired CTFR activity and chloride import into intracellular compartments [35], however, our data show that CF patients display significant HNP1-3 chlorination, thus suggesting alternative chloride-import mechanisms in neutrophils. We found significant levels of halo-HNP1-3 also in BAL from patients infected with *S. pneumoniae* and in skin abscesses from patients infected with *S. aureus*. Together, the detection of halogenated HNP1-3 in clinical samples of three different diseases where neutrophils are abundant, validate the relevance of our findings.

It reported that halogenation modulates molecular volume, pK_a value and hydrophobicity of tyrosines, therefore altering the structure, biophysical properties and functions of proteins [13]. Indeed, halogenation of HNP1 increases its surface hydrophobicity and alters its interactions with target molecules. We showed that halogenated HNP1 was more effective than HNP1 as chemokine to neutrophils and even more effectively to monocytes. Interestingly, iodination was more effective than chlorination in activating chemotaxis. These differences could be related with the intrinsic physicochemical properties and masses of the two halogen atoms (Cl 35.453 g/mol and I 126.9 g/mol) substituting the hydrogen in position 3 of the tyrosine residue, however, further studies are required to shed light on the halogen-specific effects on HNP1 activity. Moreover, halo-HNP1 were more effective in priming HMDM to produce the chemokines CCL2, CCL3, CCL4 and the anti-inflammatory cytokines IL-18bp, after a *S. aureus* infection, than HNP1. Interestingly, tyrosine halogenation did not alter the direct microbicidal activity of HNP1 toward bacteria and yeast under hypotonic conditions, the only condition known to allow direct bacterial killing effects from HNP1-3. It is noteworthy that HNP1, unmodified or halogenated, did not show cytotoxic effects under physiologically relevant salt concentration, suggesting an immunomodulatory rather than direct cytotoxic role for these peptides, as previously suggested [36].

Due to their elevated hydrophobicity, HNP1-3 form strong hydrophobic interactions with bacterial toxins and unfold them [37]. Bacterial toxins have intrinsic biophysical properties that make them extremely versatile to function in different environments. HNP1-3 share similar biophysical properties with bacterial toxins, e.g. unstructured regions and high hydrophobicity, and act as anti-chaperone, inducing unfolding of bacterial toxins trough hydrophobic binding to flexible and hydrophobic toxin regions [38]. Molecular studies demonstrated that the hydrophobic residues of HNP1-3 strongly bind the hydrophobic patches of bacterial toxins, for example to Anthrax toxin from *B. Anthacis* [39], diphtheria toxin from *Corynebacterium diphtheriae* [18], toxin B from *Clostridium difficile* [40] and others [41-43]. Our results demonstrate that tyrosine halogenation potentiates the anti-chaperone activity of HNP1 toward Anthrax toxins, LLO, PLY and in PVL. Intoxication experiments show that particularly ClY21-HNP1 is an efficient antitoxin variant compared to the unmodified peptide.

Taken together, our data show that HOCl and HOI "chemically potentiate" HNP1-3 into a more effective chemoattractant, immunomodulator and anti-toxin factor. Our data from different pathological samples demonstrate that HNP1-3 halogenation occurs *in vivo* and indicate a potential role in immune defense and pathophysiology in humans. Further studies will be necessary to evaluate other functions affected by HNP1-3 halogenation, and importantly, to harness the enhance activity of these modified peptides, for diagnosis and treatment of diseases.

MATERIALS AND METHODS

Chemicals

All reagents were purchased from common vendors of laboratory reagents for example Sigma Aldrich, Thermo Fischer Scientific or VWR Deutschland unless otherwise stated.

Isolation of human neutrophils

The ethics council of the Charité Berlin (Germany) approved blood sampling and all donors gave informed consent according to the Declaration of Helsinki. Human neutrophils were isolated by a two-step density separation as described before [43]. Peripheral blood was layered on an equal volume of histopaque 1119 and centrifuged at 800 g for 20 min. PBMCs and neutrophil layers were collected separately, washed with PBS 0,2 % HSA and pelleted at 300 g 10 min. The neutrophil pellet was resuspended in PBS 0,2 % HSA, layered on a discontinuous Percoll gradient (85 %-65 % in 2ml layers) and centrifuged at 800 g for 20 min. The neutrophil containing band was collected, washed in PBS 0,2 % HSA and pelleted for 10 min at 300 g. The cell number was determined using a CASY cell counter (OMNI Life Science).

Isolation of human monocytes and differentiation in macrophages

Monocytes were isolated by positive selection. The PBMC fraction generated during neutrophil isolation was washed in MACS buffer and pelleted 10 min at 300 g. The cells were resuspended in MACS buffer and counted using the CASY cell counter (OMNI Life Science). After subsequent pelleting, 80 µl MACS buffer and 20 µl magnetic CD14-beads were added per 10^7 cells and the mixture was incubated for 15 min at 8°C. After a washing step, the cells were passed through a magnetic LS MACS column (Miltenyi) by gravity flow. The column was washed with 8 ml of MACS buffer and bound monocytes were subsequently eluted with 5 ml MACS buffer, washed and counted. The purity of the preparation was determined by FACS staining with an anti-CD14 antibody. Monocytes were cultivated in RPMI (Gibco, Carlsbad, USA) basic medium at 37°C, 7 % CO_2. To generate monocyte-derived macrophages (MDM), monocytes were taken up in RPMI basic medium supplemented with 5 ng/ml hMCSF and incubated at 37°C and 7 % CO2 for a total of 7 days, including a medium change after three days.

Cell lines

Adherent murine (monocyte-)macrophage RAW 264.7 cells were purchased as virally transformed, immortalized oncogenic phenotypes (ATCC, Manassas, USA). RAW 264.7 were cultured in RPMI-1640 (Gibco, Carlsbad, USA) following the standard culture recommendations. The growth medium was supplemented with 10% FCS (Hyclone®, Logan, USA), 1% penicillin-streptomycin (Gibco, Carlsbad, USA), and 5 mM glutammine (Sigma, St. Louis, USA). Cell cultures were maintained below 80% confluence in TCPS flasks and passaged by incubation with divalent cation-free Dulbecco's Phosphate Buffered Saline (Gibco) prior to scraping with a rubber scraper. All cells were used at or below passage number 20 and incubated under standard conditions. Replicates are defined as cells harvested from different passages and/or flasks.

S. aureus culture

S. aureus strain USA300 was cultured by inoculating 5 mL of sterile 3% (w/v) tryptic soy broth with a single colony and incubating at 37 C for 18 h with shaking. Bacteria were harvested, washed, and then resuspended in PBS. A standard curve of absorbance at 550 nm versus colony forming units was used to approximate the bacterial concentration.

Isolation of mouse neutrophils

Mouse breeding and isolation of peritoneal neutrophils were approved by the Berlin state authority Landesamt für Gesundheit und Soziales. Animals were bred at the Max Planck Institute for Infection Biology. Mice were housed in specific pathogen–free conditions, maintained on a 12-hour light/12-hour dark cycle, and fed ad libitum. C57BL/6 mice were injected i.p. with 1 ml of 7 % Casein solution in the evening and again after 12 h at the next morning. Three hours after the second injection, mice were sacrificed by rapid cervical dislocation. The peritoneal cavity was flushed with a total of 10 ml of lavage solution and the exiting liquid with the cells was collected. The cells were pelleted by centrifugation at 200 g for 10 min and washed three times with PBS. After washing the cells were resuspended in 1 ml of PBS and mixed with 9 ml Percoll gradient. Neutrophils were separated by continuous density centrifugation for 20 min at 60000 g and the upper band containing the neutrophils was collected. Subsequently neutrophils were washed and counted in the CASY cell counter (OMNI Life Science). To assess cell purity, a cytospin with

$1x10^5$ cells was stained with Gimsa and analyzed by microscopy. Neutrophils were identified by their nuclear morphology.

Isolation of rat neutrophils

Rat breeding and blood sampling were approved by the Berlin state authority Landesamt für Gesundheit und Soziales. Animals were bred at the Max Planck Institute for Infection Biology. Sprague-Dawley rats 10-14 weeks old were sacrificed by heart puncture and 8-10 ml per animal of blood was collected. Subsequently, neutrophils were purified by an in-house negative selection kit based on a modified mouse-neutrophil positive selection kit EasySep (Stemcell Technologies). The antibodies used for the negative selection were: mouse ant-rat CD32 (Becton Dickinson), mouse anti-rat-Ly76 (Miltenyi Biotech), APC conjugated mouse anti-rat antibodies: MHC class II, CD3, CD31, CD4, CD45RC, CD49d, CD8a (Miltenyi Biotech) and CD235a (LifeSpan Biosciences). After negative selection, the neutrophil-rich pellet was resuspended in erythrocytes lysis buffer and subsequently spun down for 10 min at 300 g. To assess cell purity, a cytospin with $1x10^5$ cells was stained with Giemsa and analyzed by microscopy. Neutrophils were identified by their nuclear morphology.

Patients

All patients involved in Sepsis and ARDS Registry (SPARE-14, Hannover Medical School) were treated on the intensive care unit and were intubated for respiratory failure. Informed consent was given by the patient prior to intubation or by legal representative (#8146_BO_K_2018). BAL was performed preferably in the middle lobe or lingual or radiologically affected area. After BAL sampling, macro-impurities were removed by sample filtration through sterile gauze. BAL samples were centrifuged at 500g for 10min at 4°C and supernatant (BAL fluid) was sampled and stored at -80°C until experimental use.

Patients informed consent for the cystic fibrosis patients involved in the study: BBL01a0041; RBB07a0039; RBB07a0373; RBB07a0371; RBB07a0414; RBB07a0469S. Sputum samples from patients were collected after spontaneous expectoration or after induction with inhaled hypertonic saline (sodium chloride 6%). Sample were directly cooled and processed within 24 hours.

Patients informed consent for the *Staphylococcus aureus* skin abscess patients: EA2/003/19. Under local anesthesia the abscess was opened and taken a 4-5 mm punch biopsy under sterile conditions.

The pus was taken out of the abscess using a sterile syringe for further analysis. Furthermore, the skin gained from the punch biopsy war also used for further analysis of the surrounding abscess tissue. Healthy control samples were collected according to the approval and guidelines of the local ethics committee (EA1/0104/06).

Optical diffraction tomography and microscopy

To visualize density distributions and fluorescence, a custom-built optical setup capable of correlative Optical Diffraction Tomography (ODT, 1) and confocal fluorescence microscopy was used. A detailed description of the setup can be found in [44]. Briefly, a 532nm wavelength laser (MSL-III-532, CNI laser) was used to illuminate samples seeded on imaging dishes (81156, µ-Dish, ibidi). The complex optical fields were retrieved from spatially modulated holograms measured by illuminating samples from 150 different angles. By mapping the Fourier spectra of retrieved optical fields onto the surface of the Ewald sphere in the 3D Fourier space according to the Fourier diffraction theorem, 3D RI tomograms were reconstructed. Detailed principles for tomogram reconstruction can be found in [45-47]. Custom-written MATLAB scripts (R2020a) were used for image acquisition, field retrieval and RI tomogram reconstruction. Along with ODT images, fluorescence image stacks were acquired using a Rescan Confocal Microscope [48]. Neutrophil chromatin was visualized using SPY650-DNA (recommended dilution from manufacturer, molarity not indicated) and hypohalous acid was visualized using APF (5 µM). S. aureus cells were pre-labelled with DAPI (0.1 µM) for visualization via confocal fluorescence microscopy. For ODT a 60x water dipping objective (LUMPLFLN60XW, NA 1.0, Olympus Life Science) and a 100x oil immersion objective (UPlanFl, NA 1.3, Olympus Life Science) were used. The 100x objective was also used for the confocal fluorescence imaging.

Neutrophil lysate preparation

Cell lysates were prepared from stimulated or resting neutrophils. Cells were seeded in culture medium in 1.5 ml microcentrifuge tubes at $1x10^7$ cells/ml. After spinning down for 10 min at 300 g, cells were resuspended in RIPA buffer (Thermo Fischer) with 20 µM neutrophil elastase inhibitor GW311616A (Biomol) and Halt protease inhibitor cocktail (PIC, Thermofisher Scientific), gently mixed and incubated at 37 °C with gentle rotation. Cells were gently mixed and

centrifuged at 1000 g (30 s) to collect all residual liquid. Freshly boiled 5 X sample loading buffer (50 mM Tris-HCl pH 6.8, 2% [w/v] SDS, 10% glycerol, 0.1% [w/v] bromophenol blue, 100 mM DTT) was added to samples which were then briefly vortexed and boiled (98 °C) for 10 min with agitation and flash frozen in liquid nitrogen for storage at –80 °C. DPI and 4-ABAH inhibitors were used at concentration of 100 nM and 300 µM respectively.

Halo-tyrosine analysis

Samples and amino acid standards were acid-digested in 1ml vacuum-hydrolysis tubes in a total volume of 100µl of 4M methanesulfonic acid and 0.1% phenol for 16 hours at 110 °C. After the end of the hydrolysis the mixtures were neutralized with 4M NaOH to a pH of 3-4 and brought to a volume of 2 ml with 0.1% acetic acid. After centrifugation (10.000xg 2 min) , supernatants were passed over polymeric strong cation exchange SPE-columns (Strata-X-C 33µm, 30mg tubes, Phenomenex) which were equilibrated with 0.1% acetic acid. After washing with 2 CV of 0.1 % acetic acid, bound compounds were eluted with a 4% ammonia solution in 50% methanol. Eluates were dried in a SpeedVac evaporator and solubilized in 20µl of water.

AccQ-Tag derivatization were carried out using the manufacturer's protocol (Waters) with some modifications. In brief, the 6-aminoquinolyl-N-hydroxysuccinimidyl carbamate (AQC) reagent was reconstituted in acetonitrile at a concentration of 3mg/ml and heated at 55 °C for 2 min. 20µl of the AQC reagent were mixed immediately with 20µl of the solid-phase-extracted sample and 60µl 0.5M sodium borate pH 8.5. The mixture was incubated for 1min at room temperature followed by vortexing at 55°C for 15 minutes in the dark. 1 to 5µl of this mixture were applied to UPLC-chromatography.

Derivatized amino acids were separated by reversed phase chromatography on a AccQ-TAG Ultra C18-UPLC column (2.1 x 100mm, 1.7µm, Waters) with a linear gradient from 0.1% formic acid in 10% acetonitril to 90% acetonitrile over 6min at 55°C and a flow rate of 0.5 ml/min. Eluted compounds were detected by fluorescence (excitation and emission wavelengths at 250 and 395 nm, respectively) and by ESI-MS detection (Waters QDa). The QDa was operated in an electrospray positive ion mode by applying a voltage of 0.8 kV. The cone voltage was set at 15 V. The probe temperature was set at 600 °C. A full mass spectrum between m/z 100 and 1200 was acquired at a sampling rate of 2.0 points/sec.

Ammonium sulphate fractionation

The cell lysate was centrifuged for 15 minutes at 2500 x g, at room temperature. The supernatant obtained was centrifuged at 5000 x g for 15 minutes at room temperature to obtain clean liquids. Proteins were sequentially precipitated from 1 mL of this crude extract by stepwise addition of solid ammonium sulphate with stirring at a certain degree of saturation, followed by incubation on ice for at least 1 h and centrifugation at 10,000 x g at 4°C for 15 minutes. The pellet obtained after each centrifugation was resuspended in 1 mL of buffer containing 10 mM phosphate, pH 7. Those steps above were done for 50, 60, 70 and 80% of ammonium sulphate saturation, respectively. Aliquots of precipitated fractions were analyzed for its protein concentration and MW by 4-12% sodium dodecyl sulfate polyacrylamide gel electrophoresis (SDS-PAGE). As comparison, part of the crude extract was also directly subjected to the same analysis.

Liquid Chromatography−Mass Spectrometry Analysis (LC−MS)

For identification and relative quantification of the proteins, gel pieces were subjected to tryptic digestion, as described previously [49].

Tryptic peptides were analyzed by LC-MSMS using a Q Exactive Plus mass spectrometer (Thermo Fisher Scientific, Bremen, Germany). Peptide mixtures were fractionated by an Ultimate 3000 RSLCnano (Thermo Fisher Scientific) with a two-linear-column system. Digests were concentrated for 4min onto a trapping guard column (PepMap C18, 5 mm x 300 µm x 5 µm, 100Å, Thermo Fisher Scientific). Then, samples were eluted in 55min from an analytical column (75 µm i.d. × 250mm nano Acclaim PepMap C18, 2 µm; 100 Å LC column; Thermo Fisher Scientific). Separation was achieved by using a mobile phase from 0.1% formic acid (FA, Buffer A) and 80% acetonitrile with 0.1% FA (Buffer B). A 15 min active linear gradient from 3 to 53 % of buffer B at a flow rate of 250 nL/min was used. For 50min the Q Exactive instrument was operated in a data dependent mode to automatically switch between full scan MS and MS/MS acquisition. Survey full scan MS spectra (m/z 350–1600) were acquired in the Orbitrap with 70 000 resolution (m/z 200) after 50 ms accumulation of ions to a 3e6 target value. Dynamic exclusion was set to 10s. The 10 most intense multiply charged ions ($z \geq 2$) were sequentially isolated and fragmented by higher-energy collisional dissociation (HCD) with a maximal injection time of 200 ms, AGC 1e6 and resolution 17 500. Typical mass spectrometric conditions were as follows: spray voltage,

2.0 kV; no sheath and auxiliary gas flow; heated capillary temperature, 275 °C; normalized HCD collision energy 27%.

Additionally, the background ions m/z 391.2843 and 445.1200 acted as lock mass. Identification and relative label-free quantification of the proteins and peptides were performed with MaxQuant software version 1.6.0.1 [50] using the following search parameter set: Spectra were matched to a human (20,386 reviewed entries, downloaded from uniprot.org) or a rat (8,071 reviewed entries, downloaded from uniprot.org), a contaminant, and decoy database, enzyme: trypsin/P with two missed cleavage, static modification: carbamidomethylation (C), variable modifications: protein N-acetylation oxidation (M), dichlorination and chlorination, bromination, diiodination, triiodination and iodination (Y), mass tolerances for MS and MSMS: 10 ppm and 0.02 Da, and a calculated peptide FDR 1%.

^{36}Cl radiolabeling

Customed RMPI 1640 medium was enriched with NaCl containing ^{36}Cl radioactive isotope (25 uCi). Freshly isolated neutrophils were incubate for 1 h in the ^{36}Cl enriched buffer before adding PMA (100 nM) or live *S. aureus* (MOI 1:10) as stimuli. After 1 h of stimulation, cells were harvested and then resuspended in RIPA buffer to generate lysates. Whole lysate was analyzed by SDS- PAGE and autoradiography. The SDS-PAGE acrylamide gel was dried and exposed to a radio-sensitive film for 10 days before development.

Hypohalous acids measurement

Human neutrophils, human monocytes, mouse neutrophils and rat neutrophils were seeded onto a glass-bottomed dish and loaded with APF (5 μM) by incubation for 30 min at room temperature. Dye-loaded cells were stimulated with PMA (100 nM) or *S. aureus* (MOI 1:10). Hydrogen peroxide was used at the concentration of 1 mM. Fluorescence images were acquired twice in each experiment (before and 10 min after the stimulation with PMA) using a Leica SP8 confocal microscope coupled. The excitation wavelength was 488 nm, and the emission was filtered using a 505–550 nm barrier filter.

Phagocytosis and killing analysis

Rate of bactericidal activity of neutrophils was determined and calculated by a one step bactericidal assay [51]. Freshly isolated 1 x 10^6 neutrophils were incubated with 1 x 10^7 opsonized bacteria in 1 ml of RPMI with 0.1% human serum albumin, with final ratio of bacteria to neutrophils of 10:1. Samples were continuously rotated and incubated at 37 C and after 45 min were placed at 4 C. Neutrophils and phagocytosed bacteria were pelleted by centrifugation at 100 x g for 10 min. Supernatants were plated on TSA plates to determine the number of bacteria that were not phagocytosed. The pellets containing neutrophils and phagocytosed bacteria were washed twice with PBS and then hypotonically lysed using water at pH 11.0. After lysis, samples were pelleted by centrifugation at 300 x g for 10 min to remove the neutrophils debris and the supernatant containing the bacteria was plated on TSA plates.

UPLC and hydrophobicity analysis

Samples were dissolved in 0.1% trifluoroacetic acid (TFA) and injected onto a BEH C18 reverse phase column (2.1 mm x 100mm, 1.78µm, waters). Conditions: linear gradient from 10% to 80% acetonitrile (containing 0.1% TFA) within 6 min at a flow rate of 0.5ml at 45°C. Peptides were detected at 280nm. Nile red (Sigma-Aldrich, St. Louis, USA) was dissolved in DMSO to 0.25 mM. Varying concentrations of HNP1, ClY21-HNP1 and IY16-HNP1 were mixed in PBS, pH 7.4 with 0.2 mM Nile red. The fluorescence was monitored using a Fluoroskan Ascent fluorescence spectrometer. Measurement parameters were set to 550 nm excitation, 570–700 nm emission. Data were fitted with GraphPad/ Prism.

HNP1 peptides synthesis

Chemical synthesis of HNP1 and halogenated analogs was performed by Biosynth International, Inc. (USA, MA). Machine-assisted solid phase chemical synthesis of HNP1 and its analogs, was performed by using the 2-(1H-benzotriazolyl)-1,1,3,3-tetramethyluronium hexafluorophosphate activation/N,N-diisopropylethylamine in situ neutralization [52].

HNP1 killing assay

Bactericidal activity of HNP1, ClY21-HNP1 and IY16-HNP1 was tested against *S. aureus* USA300. *S. aureus* was maintained on trypticase soy agar (TSA) plates, and from a single colony was inoculated into 5 ml of trypticase soy broth (TSB) and cultured overnight at 37°C. The

following day, 0.1 ml of this intermediate culture was diluted with 4.9 ml of fresh nutrient broth and incubated for an additional 3 h at 37°C. A portion of this stationary phase culture was washed with 10 mM phosphate buffer, pH 7.4, and the concentration of colony-forming units (CFU) per milliliter was quantitated by measuring its absorbance at 620 nm with reference to previously determined standards. HNP1, ClY21-HNP1 and IY16-HNP1 were used at concentration 1 to 100 µg/ml in 10 mM sodium phosphate buffer, pH 7.4, or PBS, RMPI and 1-10% TSB in 10 mM sodium phosphate buffer. Control mixtures lacked HNP or contained denaturated HNPs by DTT 10 µM. After incubation with HNP for 1 h at 37°C, timed samples were removed, serially diluted, spread on nutrient agar plates, and incubated for 24 h to allow full colony development.

Candida albicans was maintained on yeast peptone dextrose (YPD) agar plates. A single colony of *C. albicans* was inoculated in 5 ml YPD broth for 18 h at 37 C. From this intermediate culture, 0.1 ml was removed and added to 4.9 ml of fresh YPD broth that was incubated at 37 C for an additional 4 h. *C. albicans* cells were washed twice by centrifugation in 10 mM sodium phosphate buffer, counted in a hemocytometer, and adjusted to the desired concentration in 10 mM sodium phosphate buffer. HNP1, ClY21-HNP1 and IY16-HNP1 were used at concentration 1 to 100 µg/ml in 10 mM sodium phosphate buffer, pH 7.4, or PBS. After incubation with HNP for 2 h at 37°C, timed samples were removed, serially diluted, spread on YPD plates, and incubated for 24 h to allow full colony development. Additionally, *C. albicansa* killing by HNP1 was measured by XTT metabolic assay as reported previously [53].

Chemotaxis

Chemotaxis was determined in triplicate samples in multiwell chambers (Abcam) using a 5 or 3 um pore size filter that separated the upper well which contained the leukocytes from the lower well which contained the putative chemotactic factors. Negative controls using the appropriate dilution buffer were run simultaneously. After 1 h incubation at 37 C, the filters were removed and stained with DRAQ5. With a microgrid, we determined the number of cells that had migrated to the lower aspect of the filter (cells/hpf) toward the putative chemoattractant, and subtracted from it the number of cells that migrated toward the diluent control. This activity was then compared with that of FMLP (neutrophils) or CCL2 (monocytes) and the results were expressed as number of cells migrated through the pores.

Cytokine profile and ELISA

Supernatant of HMDM stimulate with HNP1, ClY21-HNP1, IY16-HNP1 and *S. aureus* were harvested and incubated with the Proteome Profiler Human XL Cytokine Array (R&D), consisting of a membrane-based sandwich immunoassay. Capture antibodies spotted in duplicate on nitrocellulose membranes bind to specific target proteins present in the supernatant. Captured proteins were detected with biotinylated detection antibodies and then visualized using chemiluminescent detection reagents. The signal produced is proportional to the amount of analyte bound. ELISAs for human CCL2, CCL3 and CCL4 were conducted according to the instructions of the manufacturers. The supernatants of stimulated cells were used undiluted. For blocking of plates and dilution of standard curves, ELISA dilution buffer was used, unless it was specified differently in the instructions. ELISA plate were washed with PBS-T.

Thermostability assay

We used the Tycho NT.6 (NanoTemper Technologies) for label-free thermal shift analysis.
For each condition, 10 µL of sample were prepared in PBS at a protein concentration of 0.4mg/ml. The protein samples were loaded into UV capillaries and experiments were carried out using the Tycho NT.6. Unfolding profiles in terms of the change of fluorescence emission ratio (350/330nm) were measured over a temperature range from 35 to 95°C.

Anti-toxin experiments

Human neutrophils, primary human monocytes or RAW 264.7 cells were seeded in a 96-well plate at a density of $1x10^5$cells per well in RPMI medium 1640 containing serum. For the assay, 20 nM LF, 50 nM PA, 50 nM LLO, 50 nM PLY oand 50 nM of the PVL components LukS and LukF in equimolar ratio, and 0.1 to 10 µM of HNPs were added simultaneously to cells in serum-free RPMI medium 1640 or RPMI medium 1640 supplemented with 5% FCS. One or two hours after treatment, cell viability was determined by LDH release.

Cytotoxicity assay

To assess any toxicity of inhibitors LDH release was assessed using the CytoTox 96 Non-Radioactive Cytotoxicity Assay (Promega), according to the manufacturer's instructions. Neutrophils were seeded in RPMI in a 6 well plate with $1x10^5$ cells/100 µl. Inhibitors were

preincubated with cells for 30 min at 37 C at concentrations indicated in the figures. Assay was performed in triplicate.

LF metalloproteolytic activity

An N-acetylated, C-7-amido-4-methylcoumarin (AMC) derivative of a 14-mer fluorogenic peptide substrate (Merk) designed from the MEK-2 template was used to measure Anthrax lethal factor (LF) metalloproteolytic activity. HNP1, ClY21-HNP1 and IY16-HNP1 were test for inhibitory effect at concentration 0.1 to 10 uM. Metalloproteolytic activity of LF was monitored using a Fluoroskan Ascent fluorescence spectrometer.

Hemolysis

Briefly, red cells from normal human blood (2.5 ml) were washed four times with PBS and suspended in PBS at 5% by volume. Assays were done in 96-well plates, with a final volume of 0.1 ml/well. LLO and PLY and HNP1s were added to the wells and preincubated for 15 min on ice before adding erythrocytes (RBC). After all components were mixed, the plate was placed in a Versa Max microplate reader and incubated at room temperature for 30 min. During this time, the A700 of each well was recorded every 30 s, automatically shaking the plate before each reading. The data were plotted as ΔA700, indicating the level of protection by HNP1s.

Statistical analysis

Data are expressed as the mean ± SD and were analyzed using GraphPad Prism version 5 software. Statistical comparisons were evaluated by *t* test, and differences were considered statistically significant at $P < 0.05$.

Acknowledgements

We thank Christian Frese from the Proteomics Research Platform at the Max Planck Unit for the Science of Pathogens for proteomic analysis.

Author Contributions

AF and AZ designed the study

AF, RH, KTT, MW, AB, UAA and PF performed experiments and analyzed the data

DH, ST, AP and BS cared for the patients

AF, MR and AZ have interpreted the data and revised the manuscript for important intellectual content

AF and AZ wrote the manuscript

Competing interests

The authors declare that they have no competing interests.

References

1. Nathan C. Neutrophils and immunity: challenges and opportunities. Nat Rev Immunol. 2006 Mar;6(3):173-82. doi: 10.1038/nri1785. PMID: 16498448.

2. Winterbourn CC, Kettle AJ, Hampton MB. Reactive Oxygen Species and Neutrophil Function. Annu Rev Biochem. 2016 Jun 2;85:765-92. doi: 10.1146/annurev-biochem-060815-014442. Epub 2016 Apr 6. PMID: 27050287.

3. Klebanoff SJ, Kettle AJ, Rosen H, Winterbourn CC, Nauseef WM. Myeloperoxidase: a front-line defender against phagocytosed microorganisms. J Leukoc Biol. 2013 Feb;93(2):185-98. doi: 10.1189/jlb.0712349. Epub 2012 Oct 11. PMID: 23066164; PMCID: PMC3545676.

4. Lekstrom-Himes JA, Dorman SE, Kopar P, Holland SM, Gallin JI. Neutrophil-specific granule deficiency results from a novel mutation with loss of function of the transcription factor CCAAT/enhancer binding protein epsilon. J Exp Med. 1999 Jun 7;189(11):1847-52. doi: 10.1084/jem.189.11.1847. PMID: 10359588; PMCID: PMC2193089.

5. Hurst JK. What really happens in the neutrophil phagosome? Free Radic Biol Med. 2012 Aug 1;53(3):508-20. doi: 10.1016/j.freeradbiomed.2012.05.008. Epub 2012 May 15. PMID: 22609248; PMCID: PMC4382085.

6. Chapman AL, Hampton MB, Senthilmohan R, Winterbourn CC, Kettle AJ. Chlorination of bacterial and neutrophil proteins during phagocytosis and killing of Staphylococcus aureus. J Biol Chem. 2002 Mar 22;277(12):9757-62. doi: 10.1074/jbc.M106134200. Epub 2001 Dec 3. PMID: 11733505.

7. Green JN, Kettle AJ, Winterbourn CC. Protein chlorination in neutrophil phagosomes and correlation with bacterial killing. Free Radic Biol Med. 2014 Dec;77:49-56. doi: 10.1016/j.freeradbiomed.2014.08.013. Epub 2014 Sep 16. PMID: 25236747.

8. Lehrer RI, Lu W. α-Defensins in human innate immunity. Immunol Rev. 2012 Jan;245(1):84-112. doi: 10.1111/j.1600-065X.2011.01082.x. PMID: 22168415.

9. Eisenhauer PB, Lehrer RI. Mouse neutrophils lack defensins. Infect Immun. 1992 Aug;60(8):3446-7. doi: 10.1128/iai.60.8.3446-3447.1992. PMID: 1639513; PMCID: PMC257335.

10. Eisenhauer PB, Harwig SS, Szklarek D, Ganz T, Selsted ME, Lehrer RI. Purification and antimicrobial properties of three defensins from rat neutrophils. Infect Immun. 1989 Jul;57(7):2021-7. doi: 10.1128/iai.57.7.2021-2027.1989. PMID: 2543629; PMCID: PMC313836.

11. Nybo T, Dieterich S, Gamon LF, Chuang CY, Hammer A, Hoefler G, Malle E, Rogowska-Wrzesinska A, Davies MJ. Chlorination and oxidation of the extracellular matrix protein laminin and basement membrane extracts by hypochlorous acid and myeloperoxidase. Redox Biol. 2019 Jan;20:496-513. doi: 10.1016/j.redox.2018.10.022. Epub 2018 Nov 3. PMID: 30476874; PMCID: PMC6260226.

12. Cutting GR. Cystic fibrosis genetics: from molecular understanding to clinical application. Nat Rev Genet. 2015 Jan;16(1):45-56. doi: 10.1038/nrg3849. Epub 2014 Nov 18. PMID: 25404111; PMCID: PMC4364438.

13. Sun H, Jia H, Kendall O, Dragelj J, Kubyshkin V, Baumann T, Mroginski MA, Schwille P, Budisa N. Halogenation of tyrosine perturbs large-scale protein self-organization. Nat Commun. 2022 Aug 17;13(1):4843. doi: 10.1038/s41467-022-32535-2. PMID: 35977922; PMCID: PMC9385671.

14. Wu Z, Powell R, Lu W. Productive folding of human neutrophil alpha-defensins in vitro without the pro-peptide. J Am Chem Soc. 2003 Mar 5;125(9):2402-3. doi: 10.1021/ja0294257. PMID: 12603122.

15. Ganz T, Selsted ME, Szklarek D, Harwig SS, Daher K, Bainton DF, Lehrer RI. Defensins. Natural peptide antibiotics of human neutrophils. J Clin Invest. 1985 Oct;76(4):1427-35. doi: 10.1172/JCI112120. PMID: 2997278; PMCID: PMC424093.

16. Ganz T. Defensins: antimicrobial peptides of innate immunity. Nat Rev Immunol. 2003 Sep;3(9):710-20. doi: 10.1038/nri1180. PMID: 12949495.

17. Grigat J, Soruri A, Forssmann U, Riggert J, Zwirner J. Chemoattraction of macrophages, T lymphocytes, and mast cells is evolutionarily conserved within the human alpha-defensin family. J Immunol. 2007 Sep 15;179(6):3958-65. doi: 10.4049/jimmunol.179.6.3958. PMID: 17785833.

18. Kudryashova E, Quintyn R, Seveau S, Lu W, Wysocki VH, Kudryashov DS. Human defensins facilitate local unfolding of thermodynamically unstable regions of bacterial protein toxins. Immunity. 2014 Nov 20;41(5):709-21. doi: 10.1016/j.immuni.2014.10.018. Epub 2014 Nov 5. PMID: 25517613; PMCID: PMC4269836.

19. Kudryashova E, Seveau SM, Kudryashov DS. Targeting and inactivation of bacterial toxins by human defensins. Biol Chem. 2017 Sep 26;398(10):1069-1085. doi: 10.1515/hsz-2017-0106. PMID: 28593905; PMCID: PMC5608644.

20. Herrero-Cervera A, Soehnlein O, Kenne E. Neutrophils in chronic inflammatory diseases. Cell Mol Immunol. 2022 Feb;19(2):177-191. doi: 10.1038/s41423-021-00832-3. Epub 2022 Jan 17. PMID: 35039631; PMCID: PMC8803838.

21. Klebanoff SJ. Myeloperoxidase-halide-hydrogen peroxide antibacterial system. J Bacteriol. 1968 Jun;95(6):2131-8. doi: 10.1128/jb.95.6.2131-2138.1968. PMID: 4970226; PMCID: PMC315145.

22. Aceves C, Mendieta I, Anguiano B, Delgado-González E. Molecular Iodine Has Extrathyroidal Effects as an Antioxidant, Differentiator, and Immunomodulator. Int J Mol

Sci. 2021 Jan 27;22(3):1228. doi: 10.3390/ijms22031228. PMID: 33513754; PMCID: PMC7865438.

23. Marani L, Venturi S, Masala R. Role of iodine in delayed immune response. Isr J Med Sci. 1985 Oct;21(10):864. PMID: 4077481.

24. Simchowitz L. Interactions of bromide, iodide, and fluoride with the pathways of chloride transport and diffusion in human neutrophils. J Gen Physiol. 1988 Jun;91(6):835-60. doi: 10.1085/jgp.91.6.835. PMID: 3047312; PMCID: PMC2217627.

25. Loughran NB, O'Connor B, O'Fágáin C, O'Connell MJ. The phylogeny of the mammalian heme peroxidases and the evolution of their diverse functions. BMC Evol Biol. 2008 Mar 27;8:101. doi: 10.1186/1471-2148-8-101. PMID: 18371223; PMCID: PMC2315650.

26. Carvalho DP, Dupuy C. Thyroid hormone biosynthesis and release. Mol Cell Endocrinol. 2017 Dec 15;458:6-15. doi: 10.1016/j.mce.2017.01.038. Epub 2017 Jan 31. PMID: 28153798.

27. Shao B, Bergt C, Fu X, Green P, Voss JC, Oda MN, Oram JF, Heinecke JW. Tyrosine 192 in apolipoprotein A-I is the major site of nitration and chlorination by myeloperoxidase, but only chlorination markedly impairs ABCA1-dependent cholesterol transport. J Biol Chem. 2005 Feb 18;280(7):5983-93. doi: 10.1074/jbc.M411484200. Epub 2004 Nov 30. PMID: 15574409.

28. McCall AS, Cummings CF, Bhave G, Vanacore R, Page-McCaw A, Hudson BG. Bromine is an essential trace element for assembly of collagen IV scaffolds in tissue development and architecture. Cell. 2014 Jun 5;157(6):1380-1392. doi: 10.1016/j.cell.2014.05.009. PMID: 24906154; PMCID: PMC4144415.

29. Ulfig A, Schulz AV, Müller A, Lupilov N, Leichert LI. N-chlorination mediates protective and immunomodulatory effects of oxidized human plasma proteins. Elife. 2019 Jul 12;8:e47395. doi: 10.7554/eLife.47395. PMID: 31298656; PMCID: PMC6650281.

30. Hawkins CL, Davies MJ. Role of myeloperoxidase and oxidant formation in the extracellular environment in inflammation-induced tissue damage. Free Radic Biol Med. 2021 Aug 20;172:633-651. doi: 10.1016/j.freeradbiomed.2021.07.007. Epub 2021 Jul 8. PMID: 34246778.

31. Murphy CD. New frontiers in biological halogenation. J Appl Microbiol. 2003;94(4):539-48. doi: 10.1046/j.1365-2672.2003.01900.x. Erratum in: J Appl Microbiol. 2003;95(1):203. PMID: 12631188.

32. Müller A, Langklotz S, Lupilova N, Kuhlmann K, Bandow JE, Leichert LI. Activation of RidA chaperone function by N-chlorination. Nat Commun. 2014 Dec 17;5:5804. doi: 10.1038/ncomms6804. PMID: 25517874; PMCID: PMC4284807.

33. Jia F, Zhang Y, Wang J, Peng J, Zhao P, Zhang L, Yao H, Ni J, Wang K. The effect of halogenation on the antimicrobial activity, antibiofilm activity, cytotoxicity and proteolytic stability of the antimicrobial peptide Jelleine-I. Peptides. 2019 Feb;112:56-66. doi: 10.1016/j.peptides.2018.11.006. Epub 2018 Nov 27. PMID: 30500360.

34. Sabatino L, Vassalle C, Del Seppia C, Iervasi G. Deiodinases and the Three Types of Thyroid Hormone Deiodination Reactions. Endocrinol Metab (Seoul). 2021 Oct;36(5):952-964. doi: 10.3803/EnM.2021.1198. Epub 2021 Oct 21. PMID: 34674502; PMCID: PMC8566136.

35. Painter RG, Valentine VG, Lanson NA Jr, Leidal K, Zhang Q, Lombard G, Thompson C, Viswanathan A, Nauseef WM, Wang G, Wang G. CFTR Expression in human neutrophils and the phagolysosomal chlorination defect in cystic fibrosis. Biochemistry. 2006 Aug 29;45(34):10260-9. doi: 10.1021/bi060490t. PMID: 16922501; PMCID: PMC2931333.

36. Hancock RE, Haney EF, Gill EE. The immunology of host defence peptides: beyond antimicrobial activity. Nat Rev Immunol. 2016 May;16(5):321-34. doi: 10.1038/nri.2016.29. Epub 2016 Apr 18. PMID: 27087664.

37. Kim C, Kaufmann SH. Defensin: a multifunctional molecule lives up to its versatile name. Trends Microbiol. 2006 Oct;14(10):428-31. doi: 10.1016/j.tim.2006.08.001. Epub 2006 Aug 14. PMID: 16908156.

38. Kudryashova E, Koneru PC, Kvaratskhelia M, Strömstedt AA, Lu W, Kudryashov DS. Thermodynamic instability of viral proteins is a pathogen-associated molecular pattern targeted by human defensins. Sci Rep. 2016 Sep 1;6:32499. doi: 10.1038/srep32499. PMID: 27581352; PMCID: PMC5007486.

39. Kling C, Sommer A, Almeida-Hernandez Y, Rodríguez A, Perez-Erviti JA, Bhadane R, Ständker L, Wiese S, Barth H, Pupo-Meriño M, Pulliainen AT, Sánchez-García E, Ernst K. Inhibition of Pertussis Toxin by Human α-Defensins-1 and -5: Differential Mechanisms of Action. Int J Mol Sci. 2023 Jun 23;24(13):10557. doi: 10.3390/ijms241310557. PMID: 37445740; PMCID: PMC10341622.

40. Kim C, Gajendran N, Mittrücker HW, Weiwad M, Song YH, Hurwitz R, Wilmanns M, Fischer G, Kaufmann SH. Human alpha-defensins neutralize anthrax lethal toxin and protect against its fatal consequences. Proc Natl Acad Sci U S A. 2005 Mar 29;102(13):4830-5. doi: 10.1073/pnas.0500508102. Epub 2005 Mar 16. PMID: 15772169; PMCID: PMC555714.

41. Fischer S, Popoff MR, Barth H. Human alpha-defensin-1 protects cells from intoxication with Clostridium perfringens iota toxin. Pathog Dis. 2018 Mar 1;76(2). doi: 10.1093/femspd/fty022. PMID: 29635426.

42. Lehrer RI, Jung G, Ruchala P, Wang W, Micewicz ED, Waring AJ, Gillespie EJ, Bradley KA, Ratner AJ, Rest RF, Lu W. Human alpha-defensins inhibit hemolysis mediated by

cholesterol-dependent cytolysins. Infect Immun. 2009 Sep;77(9):4028-40. doi: 10.1128/IAI.00232-09. Epub 2009 Jul 6. PMID: 19581399; PMCID: PMC2738040.

43. Amulic B, Knackstedt SL, Abu Abed U, Deigendesch N, Harbort CJ, Caffrey BE, Brinkmann V, Heppner FL, Hinds PW, Zychlinsky A. Cell-Cycle Proteins Control Production of Neutrophil Extracellular Traps. Dev Cell. 2017 Nov 20;43(4):449-462.e5. doi: 10.1016/j.devcel.2017.10.013. Epub 2017 Nov 2. PMID: 29103955.

44. Biswas, A., Munoz, O., Kim, K., Hoege, C., Lorton, B. M., Shechter, D., ... & Reber, S. (2023). Conserved nucleocytoplasmic density homeostasis drives cellular organization across eukaryotes. *bioRxiv*, 2023-09.

45. Sung, Y., Choi, W., Fang-Yen, C., Badizadegan, K., Dasari, R. R., and Feld, M. S., 2009. Optical diffraction tomography for high resolution live cell imaging. *Optics express*, 17(1), 266-277.

46. Wolf, E. (1969). Three-dimensional structure determination of semi-transparent objects from holographic data. *Optics communications*, *1*(4), 153-156.

47. Kim, K., Yoon, H., Diez-Silva, M., Dao, M., Dasari, R. R., & Park, Y. (2014). High-resolution three-dimensional imaging of red blood cells parasitized by Plasmodium falciparum and in situ hemozoin crystals using optical diffraction tomography. *Journal of biomedical optics*, *19*(1), 011005-011005.

48. De Luca, G. M., Breedijk, R. M., Brandt, R. A., Zeelenberg, C. H., de Jong, B. E., Timmermans, W., ... & Manders, E. M. (2013). Re-scan confocal microscopy: scanning twice for better resolution. *Biomedical optics express*, *4*(11), 2644-2656.

49. Lehmann K, Schweimer K, Reese G, Randow S, Suhr M, Becker WM, Vieths S, Rösch P. Structure and stability of 2S albumin-type peanut allergens: implications for the severity of peanut allergic reactions. Biochem J. 2006 May 1;395(3):463-72. doi: 10.1042/BJ20051728. PMID: 16372900; PMCID: PMC1462689.

50. Cox J, Hein MY, Luber CA, Paron I, Nagaraj N, Mann M. Accurate proteome-wide label-free quantification by delayed normalization and maximal peptide ratio extraction, termed MaxLFQ. Mol Cell Proteomics. 2014 Sep;13(9):2513-26. doi: 10.1074/mcp.M113.031591. Epub 2014 Jun 17. PMID: 24942700; PMCID: PMC4159666.

51. Green JN, Winterbourn CC, Hampton MB. Analysis of neutrophil bactericidal activity. Methods Mol Biol. 2007;412:319-32. doi: 10.1007/978-1-59745-467-4_21. PMID: 18453121.

52. Schnölzer M, Alewood P, Jones A, Alewood D, Kent SB. In situ neutralization in Boc-chemistry solid phase peptide synthesis. Rapid, high yield assembly of difficult sequences. Int J Pept Protein Res. 1992 Sep-Oct;40(3-4):180-93. doi: 10.1111/j.1399-3011.1992.tb00291.x. PMID: 1478777.

53. Kuhn DM, Balkis M, Chandra J, Mukherjee PK, Ghannoum MA. Uses and limitations of the XTT assay in studies of Candida growth and metabolism. J Clin Microbiol. 2003 Jan;41(1):506-8. doi: 10.1128/JCM.41.1.506-508.2003. PMID: 12517908; PMCID: PMC149594.

SUPPLEMENTARY FIGURES

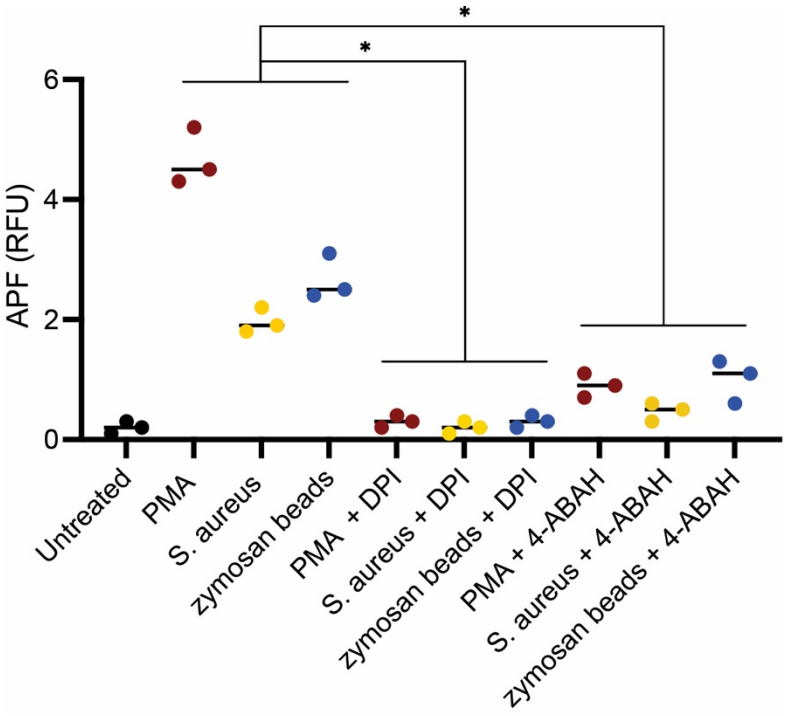

Figure S1. MPO and NOX2 inhibitors reduce hypohalous acids formation. Human neutrophils treated with diphenyliodonium (DPI) or 4-aminobenzoic acid hydrazide (4-ABAH), and stimulated with PMA, *S. aureus* and zymosan. Hypohalous acids measured by 3′-(p-aminophenyl) fluorescein (APF) at 60 min after stimulation. Bars show means ± SEM, n = 3. *$p < 0.001$, unpaired Student's t test.

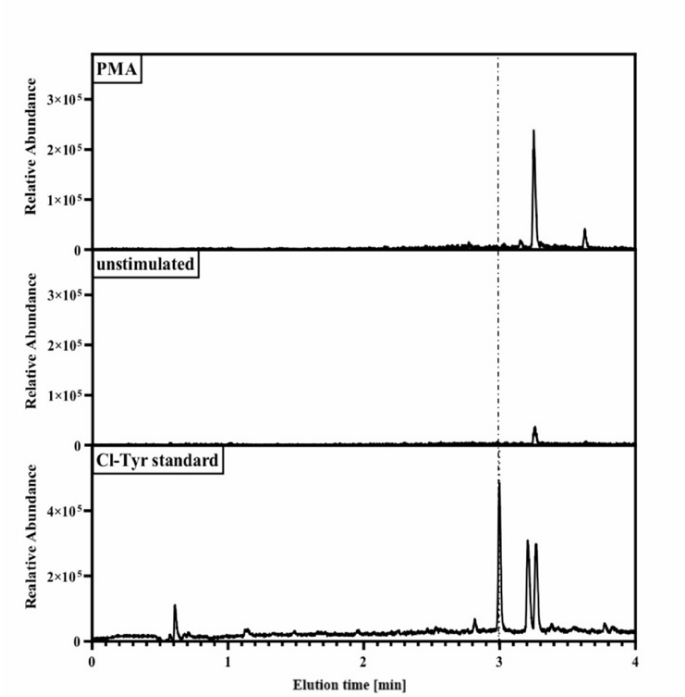

Figure S2. Chloro-tyrosine levels of non-hydrolized human neutrophil lysate. Elution profile of non-hydrolized PMA and unstimulated human neutrophils lysate measured by ESI-MS. Chloro-tyrosine standard were used as control, n=2. Dashed line corresponds with the elution of the chloro-tyrosine standard.

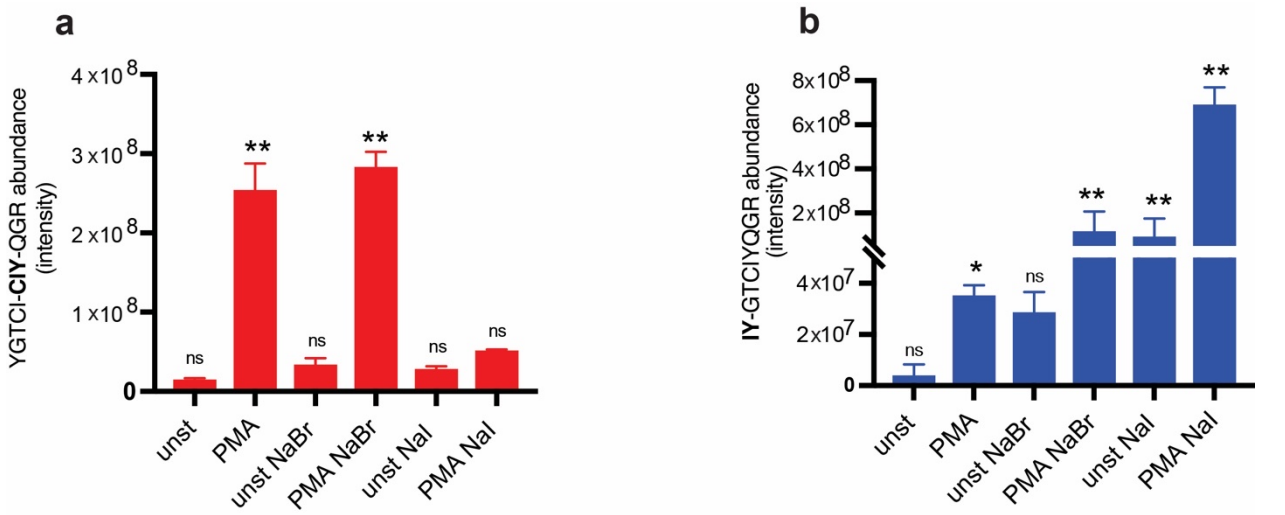

Figure S3. Proteomics analysis of halogenated proteins. Proteomic analysis of chlorinated (a) and iodinated (b) HNP1-3 derived peptides from neutrophils cultivated with supplemented halides in the medium. The supplemented halides in the medium were NaBr and NaI at the concentration of 100 µM per each. Bars show means ± SEM, n = 3. **p < 0.001, *p < 0.01, ns, non-significant unpaired student's t test.

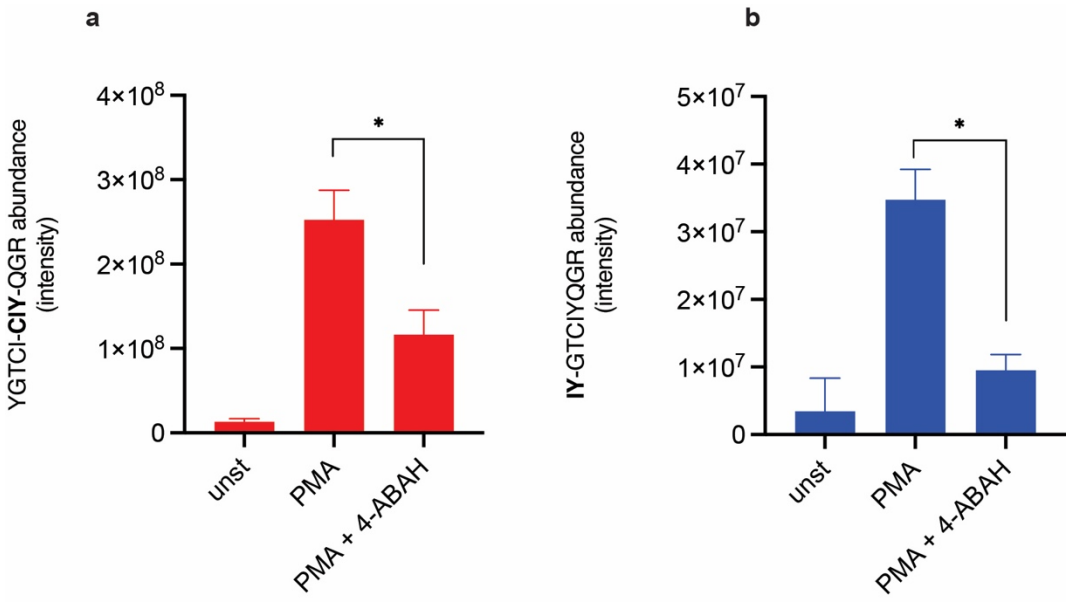

Figure S4. **MPO inhibitor reduced chlorination and iodination of HNP1-3.** Mass spectrometry analysis of chlorinated (a) and iodinated (b) HNP1-3 derived peptides from human neutrophils treated with 4-aminobenzoic acid hydrazide (4-ABAH) and stimulated with PMA. Bars show means ± SEM, n = 3. *p< 0.0001, unpaired Student's t test.

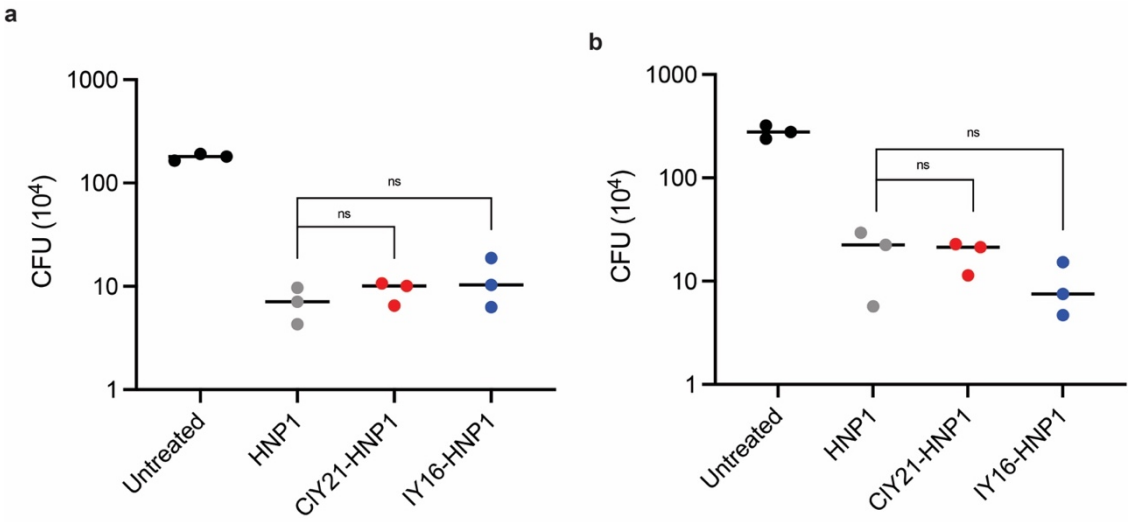

Figure S5. *E. coli* and *C. albicans* killing by halo-HNP1s. CFU count of *E. coli* (a) and *C. albicans* (b) killing using HNP1, ClY-21-HNP1 and IY16-HNP1 (50 µg/ml). n = 3; ns, non-significant unpaired Student's t test.

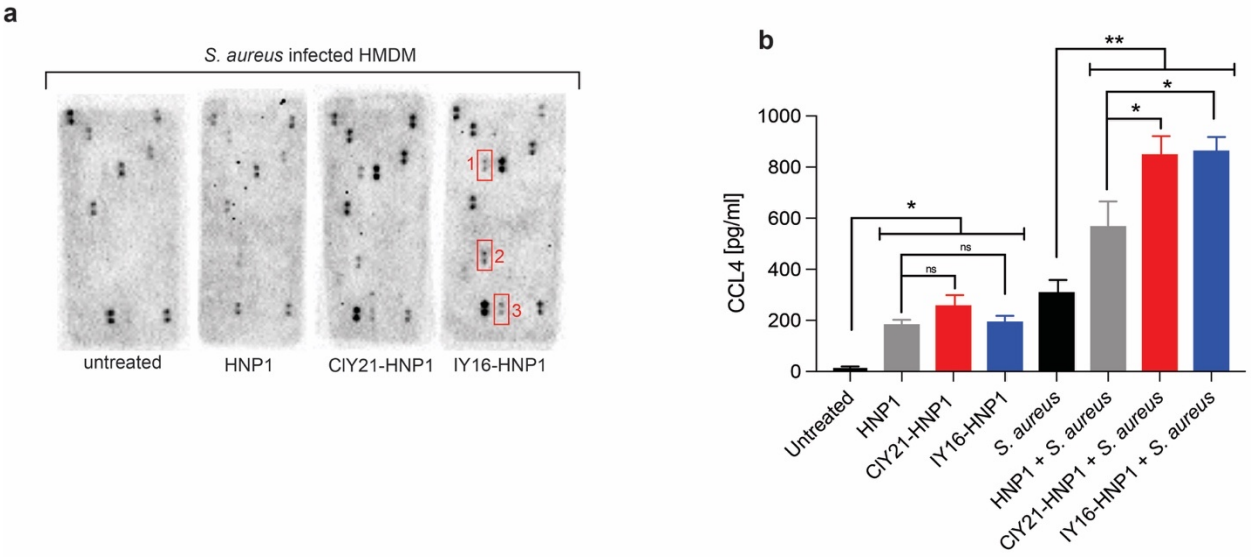

Figure S6. HNP1s modulate cytokines and chemokines production. Human cytokine profile array of HMDM infected with S. aureus and treated with HNP1, ClY-21-HNP1 and IY16-HNP1 (10 µg/ml). 1= CCL2; 2=CCL3/CCL4; 3= IL18bp. n=2 (a). ELISA of HMDM infected with *S. aureus* and treated with HNP1, ClY-21-HNP1 and IY16-HNP1 and detected levels of CCL4. Bars show means ± SEM, n = 3. **p < 0.001, *p < 0.01, ns, non-significant unpaired Student's t test (b).